《天文与地球科学杂志》

Journal of Astronomy and Earth Sciences

ChengZhu Science™

江西省诚筑环保工程有限公司主办

Serials in 2024 (12) /2024 年 12 月刊

出版人： 刘焕 香江出版社有限公司

Publisher: Liu Huan, Xiangjiang Publishing Company Ltd.

ISSN 2958-4043

Original research: Article 11. Exploring the formation of ocean current and the underlying hydrology.

Author: Liu Huan (1983-), Master of Science (First Class Honours, 2009), The University of Auckland.

DOI:10.58473/JAES0011 Retrieval from official database: www.crossref.org

Abstract: The first part of this article comprehensively reviews the relevant theories on ocean hydrology, with substantial discussion of new theories revealing the boundary layer formation process; Then representative case studies are conducted and based on the existing data that have been published, it is to re-edit these data by regression discontinuity design, which are re-analyzed with regards to the strong-wind driven current, sea-air interactions, various ocean circulation modes, ocean pollution transport and mitigation; Thirdly, this article builds up a numerical model to simulate the formation of boundary layers.

Key words: Ocean hydrology, Ocean current, Boundary layer, Ocean circulation, Ocean pollution.

This research project is formally registered via Open Science Framework (OSF) Registry, USA; Project Type: Observational Study; Project DOI: 10.17605/OSF.IO/PUQMT ; The finalization of this project is registered via OSF with DOI: https://doi.org/10.17605/OSF.IO/VHZK8

Hypothesis of research projects:

1.Does the boundary layer play an important role in the seawater hydrology? if it is, and then how it influences the dynamics of water flow?

2.Is the seawater hydrology important in the interaction between seawater and climate? If it is, and then how the seawater flow affects the climate?

3.Does the seawater boundary layer influence the ocean pollutant transport in the long-term? If it is, and then how it affects the pollution concentration distribution?

1.Introduction

The ocean (Sea) is the widest water area on the Earth's surface, which are separated by continents but organically connected to each other on the Earth. Usually the central part of the water area is called the ocean and the peripheral part is called the sea, which connect each other to form a unified water area [18].

The total area of the ocean on the Earth's surface is approximately 360 million square kilometers with an average water depth of about 3795 meters, accounting for approximately 71% of the Earth's total surface area, which contains over 1.35 billion cubic kilometers of water, accounting for approximately 97% of the total water on Earth, whereas only 2% of ocean water is available for human consumption. The four main oceans on Earth include the Pacific Ocean, Atlantic Ocean, Indian Ocean, and Arctic Ocean, where most of area are bounded by land or seabed topography lines [18]. Marine hydrology study is closely related to marine transportation, coastal protection, marine resource development, marine pollution, national defense construction, maritime medicine and rehabilitation medicine [4].

In this paper, the main study objectives include: the materials' energy transport, motion, mechanic dynamics of ocean ecosystem will be fully reviewed on the basis of the past hydrology theories, and the boundary layer mechanism discussed in my previous article is applied on the formation of turbulent flow in hydrology [1][3], with emphasis on the physical, chemical and biological exchange mechanism of ocean pollutants; Then the hydrology elements forming various types of ocean currents will be comprehensively summarized and the future research gaps is identified and filled; Finally the representative case studies that have been published in China are compared and contrasted, aiming to comprehensively analyze the methods and relevant theories necessary on the basis of published research data.

2. Review of background information

2.1.Marine hydrology

2.1.1.Marine hydrology elements and mapping

Marine hydrology elements that mainly include parameters of seawater temperature, salinity, density, ocean currents, tidal currents, waves, water transparency, water color, sea luminescence, sea ice, ocean-atmosphere interactions and etc, rely on hydrological observation at a certain geography point or section of rivers, lakes and oceans to analyze and sort out the observation data. Hydrological measurement provides necessary physical and chemical parameters of seawater such as underwater terrain measurement, water depth measurement and positioning, whose data can draw ocean hydrology maps of different ocean elements, representing the general patterns of both horizontal and vertical distribution of each element and displaying their general patterns and characteristics over time. For example, by collecting the measuring data of temperature, salinity or density of seawater, the speed of sound wave propagation in water can be calculated and estimated according to the empirical equations; Tidal observation can provide instantaneous vertical reference data for underwater terrain measurement, while wave correction can improve the accuracy of depth measurement and positioning. Consequently, these hydrology conditions can be estimated indirectly on the basis of observation parameters that are more convenient to collect [4].

Various hydrological maps add thematic elements to the geographic base map, which are indicated by using various methods. Among them, the contour line method is

commonly used to indicate the horizontal distribution of hydrological elements such as temperature, salinity, density and sound velocity, while the cross-sectional diagram is used to represent their vertical distribution; Water color chart is generally adopted by using the base color method, and tides and ocean currents are represented by different colored arrows using the dynamic line method, whose length is also used to indicate the flow velocity at different depths [4].

The temperature of seawater is a physical parameter that reflects the thermal condition of seawater, whose variation generally ranges from -2 ℃ to 30 ℃ over the world's oceans, and half of the entire ocean area displays an annual average temperature exceeding 20 ℃. The temperature of seawater shows periodic and irregular changes such as daily, monthly, yearly, and multi-year variations, which are mainly depended on the oceanic heat balance and its temporal changes. Direct observation shows that the daily variation of seawater temperature is usually very small, and the temperature varies along water depth from 0 to 30 meters, but in comparison to daily variation, the annual temperature variation along water depth can be apparent from the water depth of 0 to 350 meters. At the water depth of about 350 meters, there is a constant temperature layer, below which the water temperature gradually becomes colder with the increasing water depth (about 1°-2℃ descending per 1000 meters of depth), and when the water depth reaches 3000-4000 meters, the temperature decreases to -1℃ ~ 2℃. Sea water temperature is one of the most important factors in marine hydrological conditions, which becomes a fundamental indicator commonly used for studying the properties of water mass and describing their movements[5].

There are several factors affecting seawater temperature in seawater hydrology, mainly covering (1) Latitude: the temperature varies depending on the solar radiation obtained at different latitudes, so the distribution pattern of global seawater temperature decreases from low latitude of sea areas to high latitude of sea areas; (2) Ocean currents: along the same latitude of sea area, there is higher temperature when warm currents flow through seawater, while lower temperature is discovered when cold currents flow through seawater; (3) Season: the seawater is also significantly influenced by seasons, and usually seawater temperature is high in summer but low in winter; (4) Depth: the surface seawater decreases significantly with the increase of water depth, and there is more noticeable change within the water depth of 1000 meters, while the smaller change is usually displayed between 1000 and 2000 meters, but finally the consistently low temperature is found at the water depth below 2000 meters [5].

2.1.2.Marine hydrology measurement methods

The temperature, salinity and density of seawater can be measured both physically or chemically by equipping with the temperature-salinity depth meter, which are the three main parameters to indirectly calculate the sound velocity in seawater. For direct measurement of sound velocity in seawater, a sound velocity profiler can be used to obtain the sound velocity of the corresponding depth layer by measuring the

propagation time of sound waves at different depths and at a certain distance, thus calculating the sound velocity profile [4].

The flow velocity and direction of seawater are two dynamic factors in the development process of the seabed, which can be measured by ADCP (Acoustic Doppler Current Profile). ADCP applies the Doppler effect of ocean currents and several ultrasonic columns on calculating flow velocity and calculating flow direction based on the position of the columns. According to different working methods, ADCP can be divided into two types including stationary and mobile ones, which measure the flow velocity and direction data to draw a vector diagram of the water flow field distribution [4].

Tidal observation data value reveals the local tidal level and analyze tidal variation characteristics, providing the vertical reference surface for underwater terrain measurement, whose observation can usually include water gauge tide measurement, ultrasonic tide measurement, float tide measurement, pressure tide measurement, and GPS tide measurement[4].

After the formation of ocean currents, the continuity of seawater can lead to the formation of both upwelling and downwelling in areas where seawater diverges or gathers, which are commonly characterized and measured by the Euler method requiring simultaneous observation of ocean currents at certain stations in the ocean. Based on the measurement results, vectors representing the magnitude and direction of ocean currents are labeled, and streamline diagrams are drawn to describe the distribution of velocity in the flow field. If it is assumed that the flow field does not change over time in the long term, then the streamline represents the trajectory points of water mass in the ocean current flow diagram [7].

2.1.3.Marine hydrology and ocean current classification

According to the hydrology factors discussed above, the prevailing wind is the main driving force of ocean currents, so the larger currents in the ocean are mostly blown by strong and stable winds. ‘Wind-driven ocean current’ is directly generated by the wind, which is also named as ‘drifting’; The flow of seawater that is caused by uneven density distribution is called ‘density flow,’ also known as ‘gradient flow’ or ‘geostrophic flow’; In the process of studying ocean currents, scientists often classify them into warm currents and cold currents based on their temperature characteristics; There is also horizontal flow phenomenon of seawater caused by the tidal force generated by the moon and sun, which is called as the tidal current generated together with the tide [7].

2.2.Ocean current

Ocean currents are the water masses with different densities formed by multiple factors including thermal radiation, evaporation, precipitation, cold shrinkage, etc. In combination with wind stress, geostrophic forces, tidal forces and other effects,

relatively stable flow of seawater can be formed in large scale, as one of the common forms of seawater movement. There are many streams of ocean currents in the ocean, each of which flows along a relatively fixed route throughout the year. It is like the blood circulation of the human body, connecting the entire world's oceans and enabling them to maintain relatively long-term stability on the basis of various hydrological and chemical elements. For examples, the most famous ocean currents in the world wide are the Kuroshio Current and the Gulf Stream [7].

For the convenience of discussion, ocean currents can also be classified and named on the basis of different perspectives including the stress conditions and causes of seawater. For example, ocean currents caused by wind are called wind-induced currents or drift, while those caused by temperature and salinity variation in spaces are called thermohaline circulation; According to the force situation, ocean currents can be classified into geostrophic flow and inertial flow; Considering the different regions where ocean currents occur, there are also different ocean currents classified into sea currents, shelf currents, equatorial currents, east-west boundary currents, etc [7].

2.2.1.Ocean current measurement

There are two methods to describe the movement of seawater, including the Lagrangian method and the Euler method. The Lagrangian method is to track water mass points to describe their spatio-temporal changes, which is difficult to implement, but in modern time by using drift bottles and neutral floats, it is to track flow traces approximately characterizing the changes in flow patterns [7].

The ocean current velocity in SI units is measured by meter per second, denoted as m/s, while flow direction is represented by geographical azimuth, indicating the direction of seawater flows. For example, if seawater flows northward at a speed of 0.10m/s, the flow direction is denoted as 0°, while it is indicated by 90° for eastward flow, 180° for southward flow, and 270° for westward flow respectively. **It is worthwhile noting that the definition of ocean current flow direction is exactly opposite to that of wind direction which indicates the direction in which the wind blows.** Arrow symbols are commonly used when drawing ocean current maps, in which the length of the arrow represents the magnitude of the flow velocity and the direction of the arrow reflects the flow direction, respectively [7].

The content below tries to summarize the common types of ocean currents focusing on the hydrology elements forming and driving each type of ocean current:

2.2.2.Ocean tide current

2.2.2.1.Ocean tide formation

Under the tidal force of celestial bodies such as the sun or moon, seawater exhibits a periodic fluctuation phenomenon that the seawater rises rapidly and reaches a climax at a certain time but after some time the rising seawater is receded on its own, leaving

behind a sandy beach and experiencing a low tide. This ocean seawater cycle repeats itself endlessly in the long term fluctuation, whose movement is called as tides that are mainly caused by tidal forces imposed by celestial bodies. It manifests as tidal level rising and falling in the vertical direction, while tidal current comes and leaves in the horizontal direction [6].

There are two gravitational forces imposed on the objects of earth planet per unit mass: one is the gravitational forces on the surface objects of earth planet exerted by the moon, sun, or other celestial bodies while the other gravitational force is exerted at the center of the Earth, and the difference in both gravitational forces causes tidal force. Consequently, the magnitude of the tidal force exerted by any celestial body at a certain point on Earth surface is directly proportional to the mass of that celestial body, but inversely proportional to the square of the distance between the center of the Earth and the center of the celestial body, which is also related with the zenith angle from the celestial body to that point, and the tidal force is gradually reduced when the zenith angle is closer to 90°, whose magnitude and direction of tidal forces on Earth vary both temporally and spatially. Although the mass of the Sun is much larger than that of the Moon, its tidal force is only 46% of that of the Moon due to its distance from the Earth. Additionally, the tidal force of other celestial bodies on Earth is very small compared to the Moon or Sun, which can be ignored. The tide caused by the tidal force of the moon is called the lunar tide and the tidal force caused by the sun is called solar tide correspondingly, both of which belong to astronomical tides. Tidal forces do not only generate ocean tides, but also cause solid earth tides (earth tides) and atmospheric tides (air tides). For the ocean seawater, the solid earth tide is below the ocean tide, but the air tide is above the tide, both of which result in the impact on the ocean tide [6].

2.2.2.2.Ocean tide process

The movement modes of the moon and the sun relative to the earth display periodicity, so tides also show periodicity correspondingly. It is to describe the perspectives of periodic tidal processes below: when the tide level ascends to its peak level, it is defined as the high tide or full tide; If the tide level does not rise or fall during the period before or after this peak level, it is called a flat tide; Then the tide level begins to descend and reaches its bottom level, this critical tide level is called a low tide or dry tide; if the tide level does not rise or fall during a period of time before or after this critical level, it is called a tidal pause; Finally after the tide stops, the tide level begins to rise again for the second tide cycle. The duration of normal and stagnant tides varies, which is depended on the geographic location. For the flat tide, the middle time of the flat tide is defined as the high tide, and the height of the flat tide at that time is the height of high tide; For the tidal pause, the middle moment of the tidal pause is the low tide, and the tide height level at that time is the height of low tide correspondingly; The height difference between adjacent high and low tides is called tidal range. The periodic process from low tide to high tide is called as egre or rising tide, and the periodic process from high tide to low tide is called ebb tide. The tidal

range during the rising tide stage is called the rising tide range, and the time interval between low tide and high tide is defined as the time of rising tide; The tidal range during the ebb tide stage is called ebb tide range, and the time interval is defined as the time of ebb tide [6].

2.2.2.3.Ocean tide features

The process of tides varies from day to day due to the constantly changing positions relatively to the moon, sun, and earth, causing that not only their distances vary, but also the three celestial bodies are not on the same plane. Consequently, the tidal forces of the moon and the sun on the earth sometimes strengthen each other but sometimes weaken each other, resulting in changes in tidal height and duration, among which there are four main phenomena: unequal half moon, unequal month, unequal declination and unequal day [6].

a.Half month unequal phenomenon

On the first day of the lunar calendar month and on the fifteenth or sixteenth day of the lunar month, the positions of the moon, sun and earth are roughly in a straight line, as the tidal forces of the moon and sun are in the same direction, so the tide forces themselves to cause mutual reinforcement to each other, resulting in a maximum tidal range that occurs in every half synodic month (14.7653 days), and the corresponding tide is called a spring tide or synodic tide. After the spring tide, the tidal range gradually decreases until the first quarter (on the eighth or ninth day of the lunar calendar) or until the second quarter (on the twenty second or twenty third day of the lunar calendar) of each lunar month, when the direction of the tidal force of the moon and the sun is close to orthogonal. At this time the mutual weakening is the most significant instead of mutual strengthening, resulting in a minimum tidal range, which also occurs in every half month and the corresponding tide is called as a neap tide or square tide. The successive and alternate replacement of large and small tides is called the phenomenon of half moon inequality. In fact, the high tide in the Chinese sea area usually occurs about two days after the lunar calendar days of ‘Shuo’ and ‘Wang’, while the low tide usually occurs about two days after the upper and lower chords [6].

b.Unequal monthly phenomenon

Due to the elliptical orbit of the Moon around the Earth, it takes 27.5546 days for the Moon to go through departure from perigee, to pass through apogee, and finally return to perigee. As a result, the tidal force exerted by the Moon on the Earth also undergoes the corresponding periodic changes, and the tidal force variation in tidal range caused by this reason is called the monthly unequal phenomenon of tides [6].

c.Declination inequality phenomenon

Due to the oblique intersection between the lunar orbit and the Earth's equatorial plane, the declination of the moon constantly changes: during each lunar month, half of the month is north of the equatorial plane whereas the other half of the month is south of the equatorial plane. Because the tidal force effect is the same between the

first and second half of the month, the periodic duration is half a regression month (13.6608 days), and the corresponding tidal changes are called declination inequality phenomenon [6].

d.Daily unequal phenomenon

The phenomenon of daily variation in the height difference between adjacent high tides and low tides on the tidal curve, which goes through the circle with a period of 27.3216 days, is called as tidal diurnal variation. According to the overall effect of tidal inequality, the tidal forces can be analyzed on the basis of interaction between moon and sun motion orbits: for the moon, it passes through the equator approximately once in every two weeks, during which the inequality between adjacent high and low tides is minimal, and the corresponding tides are called equatorial tides; in comparison to the equatorial tides, when the moon is near its maximum declination in the north or south, there is significantly tidal inequality, and the corresponding tide is called the return tide. For the sun, its declination is the smallest around the vernal and autumnal equinoxes in each year. At this time if the moon just appears near the equator, then the tidal inequality phenomenon becomes the smallest due to the mutual minimization of inequality between the sun and moon, and the corresponding tide is called the equinox tide; During the summer and winter solstice, the sun's declination is at its maximum, and if the moon's declination is higher at this time, the tidal inequality phenomenon is the greatest due to the mutual maximization of inequality between the moon and sun, whose corresponding tide is called the solstice tide [6].

2.2.2.4.Main types of tidal

It is considered that tidal phenomena can be composed of many tidal components with different periods and amplitudes. Among these tidal components, the most important factors include the main lunar semi diurnal component M2, the main solar semi diurnal component S2, the lunar-solar declination daily tide K1 and the main lunar daily tide O1, with amplitudes of H_{M2}, H_{S2}, H_{K1} and H_{O1} respectively. Therefore, the ratio of the amplitudes of these four basic tidal components is usually used as to interpret and classify the characteristic value of tides [6]:

The first type of eigenvalue: $(H_{K1} + H_{O1})/(H_{M2} + H_{S2})$

The second type of eigenvalue: $(H_{K1} + H_{O1})/ H_{M2}$

According to the two eigenvalue, tides are divided into four types, including semidiurnal tides, mixed irregular semidiurnal tides, mixed irregular diurnal tides and diurnal tides, which is described below [6]:

a.Half day tide

The eigenvalue range of half day tide is that the first type of eigenvalue is less than 0.25 or the second type of eigenvalue is less than 0.5, which has two high tides and two low tides in a cloudy day with the duration of 24 hours and 50 minutes in total,

showing roughly equal heights between adjacent high tides or between adjacent low tides, such as the tides in Xiamen and Tanggu, China [6].

b.Mixed irregular half day tide

The eigenvalue range of mixed irregular half day tide is that the first type of eigenvalue ranges from 0.25 to 1.5, or the second type of eigenvalue ranges from 0.5 to 2. There are two high tides and two low tides for mixed irregular half day tide in a lunar day, but the tide heights between the two high tides or between the two low tides are different, and the tide rising and falling are also different correspondingly. The examples of this mixed irregular half day tide are the tides in Magong and Anping, Taiwan Province, China [6].

c.Mixed irregular diurnal tide

The eigenvalue range of mixed irregular diurnal tide is that the first type of eigenvalue ranges from 1.5 to 30, or the second type of eigenvalue ranges from 2 to 4, which becomes the mostly irregular half day tide within half a month, with a few days experiencing a full day tide phenomenon that only displays one high tide and one low tide in a cloudy day. The representative examples of mixed irregular diurnal tide include the tides in Yulin, Jieshi Bay, and Lingshui Bay in Guangdong Province, China [6].

d.Diurnal tide

The eigenvalue range of diurnal tide is that the first type of eigenvalue is greater than 30, or the second type of eigenvalue is greater than 4. For the diurnal tide, there are a high tide and a low tide in a single overcast day, whose duration can be more than 7 consecutive days in a lunar month. In a few days there is only a small tidal range, which exhibits the characteristics of semi diurnal tide phenomenon. The examples of diurnal tides include the tides in Beihai, Beili and Weizhou Island in China [6].

2.2.2.5.Ocean tide energy utilization

In summary, ocean tides are forced vibrations caused by tidal forces from the moon, sun and other sources, forming their own rotating tidal wave systems together with the influence of Earth's rotation and topography. Tidal energy is the ocean energy that appears in the form of potential energy, generated by the potential energy of water rising and falling of seawater tides, with theoretical reserve of tidal energy of approximately 3×10^9 kw worldwide. One of the important functions of tidal energy is to generate electricity, so many countries around the world have selected a considerable number of suitable sites for the development of tidal energy. According to the latest estimate, the tidal energy with potential for development is about 200 TW·h per year. For example, in 1912 the world's earliest tidal power station was built in Busum, Germany [6].

2.2.3.Windy ocean currents (Drift)

Wind current is the current caused by the continuous shear stress of prevailing winds

on the sea surface, and its velocity is influenced by multiple factors, including the tangential force of the wind, the vertical turbulence coefficient, and the geographical latitude of the location. Because the wind directions in the trade-wind zone, westerly wind zone, and polar easterly wind zone are relatively stable, these directional winds rub against the surface water in the ocean and the wind can transfer some of its energy to the surface seawater through friction. In addition to forming waves, it also drives the surface seawater to move, thus forming wind currents [11].

In the Northern Hemisphere, the seawater circulation that flows around the center of the subtropical high is clockwise, while the circulation that flows around the sub-polar low (mid latitude low) is counterclockwise. However, in the southern hemisphere, the circulation corresponding to the subtropical high pressure zone is counterclockwise, but both the sub-polar low pressure and polar high pressure are basically strip-shaped, so the ocean currents in those zones are parallel to the latitude circle, which means that the clockwise cyclonic circulation corresponding to the northern hemisphere does not exist in the southern hemisphere [16].

The force driven by wind firstly imposes on the sea surface, forming wind-driven ocean currents at surface layer. However, this windy ocean forces is reduced by the consumption of momentum due to the viscosity in seawater movement, so that this flow weakens with the increasing water depth until it becomes negligible at the deep water, which causes that the windy ocean current depth involved is usually only a few hundred meters, becoming a thin layer compared with the total ocean depth of several thousand meters [7].

The surface layer with a depth of less than 200-300 meters in the ocean is defined as the wind-induced drift layer. The combined forces of both wind stress and horizontal turbulent stress exerted by the planetary wind system on the sea surface, which are balanced with the deflection force of earth rotation (also named as Coriolis force), together generate wind-induced drift [7]. Coriolis parameter characterizes the displacement of a mass particle undergoing linear motion in a rotating system due to its inertia relatively to the linear motion of the rotating system, which comes from the inertia of an object's motion [8]. The magnitude and direction of wind force in planetary wind systems varies with latitude, leading to both convergence and divergence of seawater on ocean surface, whose effects can be divided into two aspects: firstly, it redistributes the density of seawater and creates the horizontal pressure gradient on the surface of wind-induced drift layer. As the wind-induced force balances with the deflection force of earth rotation, the horizontal geostrophic flow can be formed in the relatively thick horizontal layer; Secondly, at the bottom of the wind-induced drift layer in the equatorial region the seawater flows upward into the sub-surface water, or flows downward from the subsurface water, forming the ascending and descending currents in the equatorial region [7].

2.2.4.Compensating current

Due to the continuity and incompressibility of seawater, when seawater flows away from one location, seawater from the adjacent sea area also flows into this location as to supplement it, resulting in compensatory flow that displays at both horizontal and vertical directions. On the continental shelf or the ocean areas with shallow water depth, due to the significantly increased friction on the seabed or on the coast, coupled with particularly strong currents, there are complex shallow sea currents formed, such as continental shelf circulation, shallow inland sea circulation and strait currents [7]. For these types of compensating currents, current direction can be horizontal or vertical, and vertical compensation flow is further divided into two types: upward flow and downward flow [15].

For example, compared with the seawater at the middle of the sea basin, the depth of the seawater is relatively shallow at the edge of the sea basin, receiving more heat from solar radiation, so the water temperature is higher, which causes the seawater to expand and rise, resulting in lower density and higher sea level. In the middle of the sea basin, the depth of the seawater is deeper, receiving less heat from solar radiation, so the water temperature is lower, which causes the seawater to shrink and sink, leading to higher density and lower sea level. As the consequences, surface seawater flows from the periphery of the basin to the middle of the basin, while the lost seawater around the basin is replenished by the rising seawater from the seabed, forming the seawater circulation, so upwelling compensating current is commonly distributed at the edge of sea basins [15].

2.2.5.Density current

The different temperature and salinity concentration of seawater in various sea areas can cause differences in seawater density, leading to variation in seawater levels, which results in a tilt of the sea surface between two sea areas of different seawater densities and causes the flow of seawater. The ocean currents resulted in by this density driving force are called density currents. The intrusion of high-density fluids into low-density fluids is mainly caused by static pressure due to gravity and density differences. For example, the Mediterranean evaporates vigorously, resulting in higher salinity and lower water surface, while the adjacent Atlantic ocean has higher water surface, so the surface seawater of the Atlantic flows into the Mediterranean through the Strait of Gibraltar, but the Mediterranean seawater flows into the Atlantic from the bottom of the strait as the circulation [10]. Consequently, density currents usually occur together with compensating currents: when the seawater in a certain sea area flows out due to the density variation, the seawater in the adjacent sea areas comes to supplement, and the resulting ocean currents should be classified as compensating currents, which can flow horizontally or vertically. For the vertical compensating currents, they can be divided into ascending currents and descending currents. For example, the Peruvian cold current is classified as the ascending compensating current [7].

The hydrodynamics of density current is discussed in more detail as below: although

the density of seawater is determined by multiple factors including its temperature, salinity and pressure, with variation in its horizontal distribution from place to place, usually the salinity range of seawater is not large, whereas the temperature difference of seawater is large. Therefore, the density of seawater is mainly depended on the temperature of seawater. For example, in the sea area where the temperature increases due to receiving more heat from the sun, the volume of water body expands, resulting in the decrease of the density, and the sea surface (measured as isobaric surface) slightly rises; In another sea area where the density relatively increases because of less amount of solar heat received, the water temperature decreases, and the volume of water body shrinks, resulting in relatively lower sea surface (measured as isobaric surface). The equipotential surfaces of the sea surface between the two sea areas are inclined to some extent, meaning that the pressure on any horizontal plane (measured as equipotential surface) inside the seawater is not the same. Under the action of horizontal pressure gradient force, seawater flows from areas with high pressure to areas with low pressure. Once the seawater begins to flow, the Coriolis force immediately affects its motion, pulling the seawater that should have flowed in the direction of the horizontal pressure gradient to alter into the right direction in Northern Hemisphere, until the Coriolis force is equal in magnitude to the horizontal pressure gradient force but is opposite in direction. The ocean current then flows along the intersection of the isobaric and equipotential surfaces, moving at a constant speed. At this intersection line, the ocean current is exactly defined as density flow. Obviously, if the observer faces the flow direction in Northern Hemisphere, the left isobaric surface is low and the right isobaric surface is high; The density is higher on the left and lower on the right, while the water temperature on the left side is low and the water temperature on the right side is high. In the southern hemisphere, the above direction is the opposite one as counter hydrodynamics. The hydrodynamics of most powerful ocean currents in the world, such as the Gulf Stream, Kuroshio Current and Benguela Current, are all related to the distribution variation in seawater density [10].

Other factors forming density currents include the thermohaline effects of ice formation, melting, precipitation and evaporation in the ocean, resulting in uneven distribution of seawater density over a large area of the sea surface, which can cause high-density seawater to be generated in the surface layer of certain polar and high latitude sea areas, sinking into the deep and bottom layers. Under the effect of horizontal pressure gradient force, the high-density seawater flows horizontally in the deep layer, which subsequently flows upwards through the middle layer from the water bottom layer to the surface layer, forming the oceanic thermohaline circulation [7].

The wind drift generated on the surface of the ocean constitutes the wind-driven circulation on the surface of the ocean. For example, the North Equatorial Current at low latitude and the South Equatorial Current located at mid latitudes are blocked by the coast at the western boundary of the ocean, causing their main currents to turn north and south respectively. Due to the variation of Coriolis parameters with the

change of latitude (β - effect) and the effect of horizontal turbulent friction, these wind drift forms the strengthened ocean westward flow with narrowed flow spokes and increased flow velocity [8]. Half of the total heat energy transferred from the equatorial region to the high latitude regions of the Earth in each year is carried by these westward strengthening flows along the western boundary of the ocean. The velocity of thermohaline circulation entering the upper layer of the ocean increases in the northern hemisphere due to its direction that is the same as the westward strengthening flow of the ocean. In comparison, due to the opposite direction and slower flow velocity, the westward strengthening influence on ocean circulation in the southern hemisphere is not very significant [7].

For another example, the wind-driven circulation in the mid latitude and high latitude regions of the southern hemisphere on the ocean surface forms an Antarctic Circumpolar Current that continuously flows around the Antarctic continent due to the absence of continental coastal barriers [7].

In the eastern and nearshore waters of the ocean, the wind blows uniformly, which is almost parallel to the coast for a long time, so that the wind drift is generated and horizontal convergence and divergence of seawater occurs, resulting in both upwelling and descending currents; Concurrently, due to the accumulation and loss of seawater near the coast, the sea surface tilts and the force of horizontal pressure gradient occurs, resulting in coastal currents and forming both upwelling and downwelling streams along the coast [7].

2.2.6.Cold current and warm current

Ocean currents generated by the temperature variation can be divided into two types: cold currents and warm currents, which is depended on whether their water temperature is lower or higher than the water temperature of the sea flowing through. The cold current comes from areas with lower water temperatures, while the warm current comes from areas with higher water temperatures. The horizontal flow velocity of ocean currents ranges from a few centimeters per second to 300 centimeters per second at the surface layers, while the horizontal flow velocity at deeper water depths is less than 10 centimeters per second. The vertical current velocity is very slow compared with horizontal flow, ranging from a few centimeters per day to several tens of centimeters per hour [7].

2.2.7.Geostrophic flow

Geostrophic flow is the stable ocean current when the forces are balanced between the horizontal pressure gradient and horizontal geostrophic force in the ocean area where the turbulent frictional force can be ignored [7]. Geostrophic current can be also defined as the the ocean current occurring in the deep ideal ocean where the horizontal pressure gradient force generated by the uneven distribution of seawater density is balanced with the horizontal geostrophic deflection force, ignoring the effect of turbulent frictional forces. These two different directional forces

continuously change the direction of seawater flow, which leans to the right at the northern hemisphere and leans to the left at the southern hemisphere, until both the horizontal pressure gradient force and the Coriolis force reach equilibrium, and then the flow reaches stability [12].

There are mainly four characteristics with regards to the geostrophic current: the magnitude of the geostrophic flow velocity is directly proportional to the tangent of the angle between the isobaric and equipotential surfaces, but is inversely proportional to the Coriolis parameter; Flowing along the intersection line of two sides (one side is isobaric surface and the other side is equipotential surface), the flow direction in the northern hemisphere is 90 degrees to the right of the horizontal component of the pressure gradient force; In the Northern Hemisphere, when it is to face the direction of flow, the isobaric surface is higher on the right but lower on the left; The inclination of the isobaric surface caused by the internal pressure field is mainly reflected in the upper layer of the ocean and decreases with the increasing depth, whereas the inclination of the isobaric surface caused by the external pressure field directly reaches the seabed from the ocean surface [12].

For example, one of the representative theory is the Ekman Drift forming at the surface ocean layer, driven by three kinds of natural force: wind force, horizontal geostrophic deflection force (Coriolis force) and friction force from deeper water layer. The flow direction of surface seawater is 45 degrees away from the wind direction in theory, with the rightward deviation in the northern hemisphere and the leftward deviation in the southern hemisphere. When surface seawater begins to flow under the effect of wind shear stress, the Coriolis force immediately imposes on it, causing the direction of wind current flow to be inconsistent with the wind direction. Due to the fact that the direction of the Coriolis force in the northern hemisphere is biased to the right of the direction of object motion, and in the southern hemisphere it is biased to the left of the direction of object motion, the flow of wind currents is biased to the right of the wind direction in the northern hemisphere and to the left of the wind direction in the southern hemisphere, respectively. In addition to the shear stress and Coriolis force of the wind, the surface seawater flow is also affected by the internal friction force between surface water and the deeper seawater. Therefore, the factor determining the magnitude of the wind current and wind direction deviation angle is the balance of these three forces [13]. As the depth increases, the angle of deviation from the wind direction becomes larger, but the flow velocity decreases accordingly. When it reaches a certain depth, the direction of drifting is exactly opposite to the direction of surface drifting currents, with a flow velocity of only about one twenty third of the surface flow velocity, and then this critical depth is called the frictional depth in oceanography. Therefore, it is usually considered that Ekman Drift is only formed at the surface layer of seawater flow within the range of friction depth (usually about 500m of water depth), whereas the current velocity below this friction depth is slow, which can be ignored [16].

Although Ekman Drift is a kind of idealized ocean current, it can approximately reflect some of the motion laws of seawater in theory. For example, the ocean currents in the thicker lower layers of the ocean are similar to geostrophic currents only, whereas in the thinner and upper layer of the ocean, there are both geostrophic currents and Ekman drift, both of which become the fundamental flows of the ocean [12].

2.2.8.River discharge

River discharge current is the flow of seawater caused by river runoff into the sea near the estuary [7].

2.2.9.Rip current

The rip current propagates from the open sea to the coast and is generated when the wave breaks in the wave breaking zone, moving from the shore to the deep water direction [7]. Consequently, rip current is the narrow and strong flow moving from the coast into the sea, which flows outwards in the direction perpendicular to the coast. The narrow width of rip flow generally does not exceed 10 meters and its length is usually between 30-50 meters, sometimes reaching up to 700-800 meters. Although this stream of rip flow is not long, its speed can be very fast, with a flow rate of over 2 meters per second. The duration of each stream is usually two to three minutes, and sometimes can be even longer, so it can quickly drag people into the water. Rip current often occurs at the interruption of white waves, beach gaps or low-lying areas, rocky areas, which are perpendicular to the trenches of coast, pocket shaped coasts, etc [14].

The formation of rip flow can be explained as below: waves spread to the shore, or winds blow towards the shore, which may form the buildup of seawater on the shore firstly, subsequently leading to the backflow of seawater offshore. The returning seawater gathers in areas with small waves near the coast and then turns towards the sea along a narrow band, resulting in considerable flow velocity. For example, the most common case is when water breaks through the obstruction of sandbars. The sandbar is the narrow sand dune that accumulates along the outer side of the coast. Seawater usually clusters on the lower surface inside the sandbar, but in some cases, the receding water flow can generate sufficient backward pressure to form a breakthrough in certain parts of the sandbar, immediately forming the rip current with narrow width and strong velocity [14].

2.2.10.Longshore current

Compared with rip current, longshore current direction is the current parallel to the coast, which is generated when waves propagate from the open sea to the coast and break up in a fractured zone [7].

2.2.11.Summary of ocean current types

In summary, the actual ocean currents that occur are always the result of a

combination of multiple factors, among which the main cause of ocean currents is the variation in wind speed and seawater density. In addition to tidal movements caused by tidal forces, seawater flows on a large scale along relatively fixed paths in the ocean, whose driving forces that cause ocean currents to move commonly include wind or the uneven distribution of seawater density caused by the thermohaline effect. For the thermohaline driving force, the seawater flows horizontally in a regular direction, which are classified into warm currents and cold currents according to the water temperature. Generally, ocean currents flowing from low latitudes to high latitudes are likely to become warm currents, while ocean currents flowing from high latitudes to low latitudes are likely to become cold currents; Ocean currents can also be classified into wind-driven currents, density currents, and compensating currents based on their causes. The prevailing wind blows over the sea surface, pushing the seawater to drift with the wind and causing the upper seawater to drive the lower seawater to flow, which forms a large-scale ocean current called wind-induced ocean current, and the ocean systems on the surface of earth planet are mostly composed of wind-driven currents [7].

2.3.Meso-scale vortex and circulation

The westward strengthening current of the ocean flows northward in the northern hemisphere (or southward in the southern hemisphere correspondingly), then turning eastward. When it reaches the specific area, the flow becomes unstable, and the axis of the current mapping bends in wave shape near its average position, resulting in the bending (or meandering) of ocean currents. Finally, it forms the circular flow and separates from its parental streams, generating a cold current ring with cold water from the continental shelf and a warm current ring with warm water from the ocean interior, which becomes a type of meso-scale vortex with medium scale. In addition, in other parts of the ocean, due to the instability of ocean currents, other types of meso-scale eddies can also be formed. These meso-scale eddies concentrate significant amount of energy on the ocean, forming various weather like eddies that stack over the ocean's climate like average circulation field, making ocean circulation more complex[7].

In the continental shelf or shallow waters of the ocean, due to the significant friction between the coast (or the seabed) and strong currents, complex shallow sea currents such as continental shelf circulation, shallow inland sea circulation and strait currents are formed [7].

2.3.1.Overall pattern of ocean surface circulation in Earth

There are various current circulations on the surface of ocean in our planet, mainly including the anticyclonic oceanic circulation centered around the subtropical high in mid to low latitude sea areas, the cyclonic oceanic circulation centered around a low-pressure area in the mid to high latitudes of the Northern Hemisphere, the westerly drift in the mid latitude sea area of the southern hemisphere, the circumpolar circulation formed around the Antarctic continent, and the monsoon circulation

formed in the northern Indian Ocean [8].

2.3.2.Anticyclonic oceanic circulation

Under the influence of the trade-wind belt, the trade-wind drift, including both South and North Equatorial Warm Current, flows westward. When the drift encounters the continent, a portion of the seawater turns back due to the uneven north-south velocity components of the trade-wind drift that yields shearing stress and compensation effect, forming equatorial counter current/back flow and equatorial subsurface current from west to east as anticyclonic oceanic circulation, while another portion of the trade-wind drift moves towards the north and south of high latitudes, forming the Kuroshio Current in the North Pacific, the East Australian Current in the South Pacific, the Brazilian Current in the South Atlantic, the North Atlantic Gulf Stream in the North Atlantic, and the Mozambique Current in the South Indian Ocean [8].

Under the influence of the westerly wind belt, westerly winds drift eastward and diverge into high latitude and low latitude currents on both sides upon encountering continents, consequently forming compensating currents as anticyclonic oceanic circulation. The ocean currents flowing towards low latitudes include the California Current in the North Pacific, the Peru Current in the South Pacific, the Canary Current in the North Atlantic, the Benguela Current in the South Atlantic, and the Western Australian Current in the South Indian Ocean [8].

In summary, there are the compensating currents commonly including trade-wind drift, trade-wind drift turning towards high latitudes after encountering continents, westerly drift, and westerly drift turning towards low latitudes after encountering continents, which are classified into the anticyclonic ocean circulation in the subtropical sea areas of various oceans. These oceans cover the following sea areas of the ocean: North Pacific, South Pacific, North Atlantic, South Atlantic, and South Indian Ocean [8].

2.3.3.Cyclonic ocean circulation

The cyclonic ocean circulation from the mid to high latitude of sea areas in the Northern Hemisphere is composed of compensating currents formed by the westerly drift that encounters land and splits northward, as well as the ocean currents formed by polar easterly wind belts on the west coast from the mid to high latitude ocean [8].

The ocean current circulation in the North Pacific includes the North Pacific Warm Current, Alaska Current, and Kuril Current, while in the North Atlantic, there are the North Atlantic Warm Current, Norwegian Warm Current, and East Greenland Cold Current [8].

The North Indian Ocean monsoon drift is influenced by two types of wind driving forces: the first wind force is the South Asian monsoon, with the northeast monsoon prevailing in the half year of winter, forming the northeast monsoon drift, and the other wind driving forces is the southwest monsoon prevailing in the other half year

of summer, forming the southwest monsoon drift [8].

2.3.4.Antarctic Circumpolar Circulation

Under the blowing of the polar easterly wind belt, the Antarctic circumpolar circulation is formed around the Antarctic continent, and then a westerly drift is formed around the Antarctic continent in the lower latitude direction. Due to the consistent natural characteristics of this sea area, the outer sea area of Antarctica is sometimes named as the 'Southern Ocean'[8].

2.4.Function of ocean current in earth ecosystem

Ocean currents lead to the impact and constraint on various physical, chemical, biological and geological processes in the ocean, which also affect the formation and changes of climate and weather over the ocean [7]. The overall importance of ocean currents, which play the role in Earth ecosystem, is firstly to transfer thermal energy from multiple ocean regions to other different ocean areas, balancing thermal energy, then to transfer nutrients from multiple oceanic regions to other different oceanic areas, and finally to distribute seawater with different oxygen contents from multiple ocean regions to other ocean areas due to the motion of ocean currents [8]. My another paper has discussed that the terrestrial vegetation is the main source of providing oxygen in our earth planet [17], and the atmospheric oxygen should become the soluble oxygen in ocean water by the mixture effects of wind, sea wave and precipitation, supplying the compulsory survival condition for ocean creatures. This oxygen process among terrestrial vegetation, atmospheric oxygen, and soluble oxygen of ocean is discussed in detail in Figure 2 below.

2.4.1.The effects of ocean current on climate

For example, warm currents result in the warming and humidifying effect on coastal climate, whereas cold currents cause the cooling and dehumidifying effect on coastal climate; In the sea area where cold and warm currents intersect, the disturbance of seawater can bring nutrients from the lower layer to the surface layer, which is conducive to the large-scale reproduction of fish and provides bait for them; Both warm and cold currents can also form a kind of 'water barrier', hindering fish activity and concentrating fish populations, which is beneficial to form large-scale fishing grounds such as the Newfoundland fishing ground and the Hokkaido fishing ground in Japan [7].

The effect of ocean currents on precipitation and fog differs between warm and cold currents: heat and water vapor are transported upwards over warm currents, resulting in unstable stratification and increasing air humidity, which leads precipitation more likely to occur, whereas the cold current generates temperature inversion, so the stratification is stable and the water vapor is not easily transported upwards with weaker evaporation. Although the relative humidity in the lower layer is sometimes high over the cold current, it can only form fog without sufficient meteorological conditions forming rain. The surface of the cold current is often covered with

advection fog, classified into sea land wind fog and sea fog. When sea land wind fog meteorological condition occurs, land wind flows to the surface of the cold current during the day and forms advection fog. In comparison, sea fog meteorological conditions is different from sea land wind fog, under which wind blows from the surface of the warm current to the surface of the cold current, forming advection fog at the confluence of both warm and cold currents [8].

Overall, the temperature and humidity is increased in the atmosphere of warm currents, while temperature and humidity is decreased in the atmosphere of cold currents. The influence of ocean currents on atmosphere temperature causes the transfer of heat from low latitudes to high latitudes, especially converted by the warm currents. However, for the same latitude, the effect of ocean currents on temperatures at both sides of continents is that warm currents pass through the coastal areas of continents with higher temperatures, while cold currents pass through the coastal areas of continents with lower temperatures [8].

2.4.2.Effects of ocean currents on marine organisms

For example, some sea areas are affected by offshore winds, and the upwelling of deep seawater brings a large amount of nutrients to the surface, forming fishing grounds such as the Peruvian fishing grounds [7]. This nutrition transport particularly occurs in the areas where the warm and cold currents intersecting causes disturbance to the seawater. The four famous fishing grounds in the world and their ocean currents include Hokkaido Fishing Ground located near Hokkaido Island, Japan, where the Japanese Warm Current and the Kuril Cold Current intersect; North Sea Fishing Ground located in the European North Sea, where the North Atlantic Warm Current and the Arctic East Wind Belt bring cold water southward from the Arctic Ocean; Peruvian fishing grounds where Southeast trade winds prevail along the coast, which are offshore winds that cause upwelling compensating currents; Newfoundland Fishing Ground located near Newfoundland Island, Canada, where the North Atlantic Warm Current and Labrador Cold Current intersect. Especially for another example, penguins species habitat in the Equatorial Region, which is distributed in the Colon Islands (also known as the Galapagos Islands) in the eastern Pacific Ocean, is also established naturally due to the Peruvian cold wave [8].

2.4.3.Ocean currents and sailing

Ocean currents influence the sailing and shipping transportation in the ocean, and usually sailing along ocean currents can save fuel and accelerate speed, but when warm and cold currents meet, sea fog is often formed, which is unfavorable for maritime navigation. In addition, the Arctic Ocean carries icebergs southward from the Arctic region, posing a significant threat to maritime navigation [7].

2.4.4.Ocean currents and environmental pollution

Ocean currents can also diffuse pollutants from nearby waters to other areas, which is beneficial for the diluting of pollution and accelerates the purification process, but as

a result other sea areas may be contaminated as well, expanding the scope of pollution [7].

2.4.5.Ocean currents and electricity

In ocean motion, ocean currents do not only play an important role in the climate and ecological adjustment to achieve eco-balance of the Earth, but also can drive turbines to generate electricity and deliver green energy to people. The ocean currents follow the certain route and move repeatedly, with the scale that is thousands of times larger than the giant rivers and streams on Earth land, so the potential energy being capable of utilization is considerable. For example, among all the ocean currents there is a very large scale ocean current that can be called as 'giant' in ocean currents, which is the famous 'Gulf Stream' with width of 60-80 kilometers and thickness of 700 meters, and its total rate of flow is from 74 to 93 million cubic meters per second. This total flow is nearly twice as large as the Kuroshio Current in the North Pacific that is the world's second largest ocean current, and is even more than 80 times the total flow amount of all rivers on Earth land [7].

Consequently, understanding the motion orbits of ocean currents, the mutual interactions between large-scale sea air and long-term climate change are of great significance for fisheries, shipping, pollution control and military affairs [7]. In summary, ocean currents play an important and positive role in balancing and driving the Earth's biosphere and abiotic (both chemical and physical) environment, providing positive assistance not only for the survival of most marine organisms, but also for those on land [8].

2.5.Representative current

2.5.1.Kuroshio Current

The Kuroshio Current is the strongest ocean current in the Pacific region, named due to its deep blue color and black appearance. Compared with the sea area which it flows through, it displays the characteristics of high temperature and high salinity, which is hence called the Kuroshio Warm Current as well. There are several streams divided when the Kuroshio Current enters the East China Sea. According to its traditional definition, the Tsushima Warm Current runs north along the west coast of Kyushu, west of Amami Oshima Island. When the Kuroshio Current goes through the south of the Goto Islands, it splits into two streams: the main stream flows northeast through the Korea Strait into the Sea of Japan, while the western stream enters the South Yellow Sea through the south of Jeju Island, forming the Yellow Sea Warm Current. The Kuroshio Current is divided into two streams in the southeastern water of Taiwan. The mainstream heads northwards, and the other stream flows northwest into the Bashi and Balintang Strait (the western branch of the Kuroshio Current), which then splits into two streams in south of Taiwan: the larger stream flows southwest into the South China Sea, forming part of the winter circulation in the South China Sea, while another small stream enters the Taiwan Strait and heads north along the eastern side of the strait [7].

The Kuroshio Current is known due to its strong flow velocity, narrow flow amplitude and large thickness. The flow rate is generally 1-3 knots, reaching 3.5 knots at east of Suao. After entering the East China Sea, the flow velocity decreases slightly to approximately 1-2 knots, but the flow velocity increases again, reaching 2.5 -3 knots at the location around 26° N & 126° E and even up to 3.4 knots at southwest of Yakushima Island. On the cross-section of flow velocity, the Kuroshio Current is often consisted of two flow cores northward or northeastward, separated by a reverse flow core. The stronger flow core is located near the coast, indicating the strengthening of the oceanic circulation towards the west coast. However, in the vicinity of Okinawa and Amami, the Kuroshio Current often generates backflow on the right side of its main stem, due to the friction with the terrain, but this counter current velocity is not large, about 0.3-0.5 knots, and the thickness is relatively shallow, with an average flow rate of only approximately 1/5 of the mainstream [7].

The Kuroshio Current shows the relatively narrow range, with the averaging range of less than 100 nautical miles, and the strong current zone with more than 2 knots is only 25 nautical miles. The thickness of the Kuroshio Current is about 800 meters, which can be divided into four water layers from top to bottom: surface water, subsurface water, middle water and deep water. Although the Kuroshio is a stable and powerful ocean current, there is significant change in flow velocity, flow rate and amplitude. Moreover, the flow axis of Kuroshio Current also swings and bends along the current orbit. With variation in time, there are various cycles including long, medium and short cycles, and from the spatial perspective there is medium to small-scale change in spaces as well. To the east of Taiwan, the northward flow and velocity of the Kuroshio Current exhibits a six-month cycle, with the maximum velocity in spring and autumn (at the velocity of 120 cm/s) and the minimum velocity in winter and summer (at the velocity of 50 cm/s), respectively. In addition, there are several cold and warm eddies appearing on both sides of the Kuroshio Current [7].

2.5.2. The hydrology environment of Philippines Sea

The map of Temperature-Salinity point clustering in the sea area of Kyushu Palau Ridge displays as an inverse ‘S’ shape on the graph, which is roughly divided into four types according to the temperature and salinity structure: surface high temperature and low salinity water (HTLS), subsurface high temperature and high salinity water (HTHS), mid-level low temperature and low salinity water (LTLS), and deep low-temperature and low salinity water (LTHS). The Temperature-Salinity points in the surface, subsurface, and mid-level are discrete, indicating strong mixing of seawater in these depth levels. The surface high temperature and low salinity water are located at depths of 0-50m with the highest water temperature (28 ℃ -30 ℃) that is attributed to solar radiation on surface, but the lowest salinity (33.5 ‰ -34.5 ‰) is found at this depth, which is attributed to the dilution effects by surface precipitation; The secondary layer of high-temperature and high salinity water is located at the depth of 100-200m (24 equipotential density surface), where water temperature

(15 ℃ -28 ℃) is lower than it at the surface layer, but the highest salinity (34.7 ‰ -35.3 ‰) is reported at this depth; Middle level low-temperature and low salinity water is located at the depth of 300-1000m, with water temperature (4 ℃ -16 ℃) higher than deep layers, but there is seawater with lower salinity (34.1 ‰ -34.5 ‰); Deep low-temperature and low salinity water is located at depths of over 1000m, and the lowest water temperature is less than 5 ℃, with the salinity ranging from 34.5 ‰ to 34.7 ‰ [19].

The Northeast trade winds prevail long-termly in low latitude regions of the Northern Hemisphere, coupled with the influence of geostrophic force tending to the right direction, which forms the Pacific North Equatorial Current flowing from east to west in the 8° N-20° N of sea area. This equatorial current crosses the Pacific Ocean, mainly flowing through the southern part of the Philippines, where the horizontal flow amplitude is about 2000km and the vertical flow amplitude is about 250m, with the average horizontal flow velocity of about 0.4m/s and constant vertical flow velocity at 0.1m/s, respectively. In the flow area of this equatorial current, the flow velocity near the equator is relatively high, reaching 0.55m/s in the southern Philippines, which provides the dynamic conditions for the consistency in both temperature and salinity structure of Philippine Sea, especially in the 10° N-20° N of sea area [19].

From the equator to 3° N, the Pacific South Equatorial Current is formed, featured by an average flow velocity of about 0.3m/s and a water depth of about 200m (0.1m/s isokinetic line). On the equatorial windless zone located at the south of the North Equatorial Current, Pacific Ocean, there is a west to east ocean current known as Equatorial Counter Current (NECC) passing across the Philippine Sea between the South and North Equatorial Currents. Analysis shows that the equatorial cross-section of southern boundary of this counter current (NECC) is located at about 3° N, and the northern boundary is about 5° N. The water depth of this equatorial counter current is below 500m, with the maximum flow velocity reaching 0.6m/s, but the subtropical counter current is weak or even no longer apparent. It should be noted that the North Equatorial Current and Kuroshio Current may lead to significant impact on the east-west distribution of both temperature and salinity structures in the sea areas, showing significant variation between south of 10° N and north of 20° N [19].

Overall, the ocean currents in the Philippine Sea are mainly distributed as a band-pattern in shallow water depth below 500m, and especially in shallow water below 200m, where the flow velocity is significantly affected by ocean current dynamics. The current velocity at a depth of 500m significantly slows down, especially with the disappearance of the North Equatorial Current. The sea area at north of 20° N is mainly consisted of the afterflow of Kuroshio Current and weaker subtropical counter currents, while both equatorial currents and western boundary currents are present with significantly increased flow intensity in the South China Sea below 20° N. Both the vertical and horizontal distribution of these currents may be the

main driving factors causing significant regional differences in temperature and salinity structures at the upper layer of shallow water depths below 500m [19].

In summary, Philippine Sea exhibits significant differentiation in hydrological environment with dynamic configuration characteristics. The marine hydrology is characterized in horizontal and vertical distribution separately: the horizontal distribution of both temperature and salinity structures shows a differentiation pattern of five zones, in which the north-south boundary is located at approximately 20° N and 10° N, and the east-west boundary is located at approximately 137° E, showing significantly regional differences; The vertical distribution follows a pattern of 'three lines and one circle': at the water depth of 200m as the boundary, the upper layer exhibits significant seasonal variations and distinct regional characteristics, while the lower layer shows less seasonal variation, but the temperature and salinity structure at water depths of 200-500m shows an inverse distribution pattern compared with the upper layer. At deeper layers, the temperature and salinity structure at depths below 500m changes little without significant difference, and there is the sub-layer with low temperature and low salinity at water depths of 500-1000m in the sea area north of 20° N [19].

3. Original discussion and research gaps in ocean hydrology

The process of the boundary layer formation at each substance state (gaseous, liquid, solid) can be modeled by 3D modeling technology discussed in my another article [2], and the preconditions of boundary layer formation should include two conditions: one is that the spatial variation in substance's density and composition should reach the threshold, which is reflected by the variation along the spatial scale of modeling; the other is that the relative speed of substance motion is low enough to form boundary layers, which is measured by the variation along the temporal scale of modeling. The higher variation per spatial scale and lower variation per temporal scale in this 3D modeling would tend to form boundary layer more efficiently. The higher spatial variation in substance density and composition will facilitate magnetization between different substance layers, initiating boundary layer formation as discussed in my article [3], while the less temporal variation in substance density and composition reflects the lower relative speed of fluid substance's motion, increasing the sink effects of fluid substances on the boundary layer, which consequently enhances the stability of substance boundary layers. Consequently, this boundary layer formation sub-model would fill in the research gaps in 3D modeling in atmospheric, geological and hydrology environment, which will be firstly discussed in this hydrology paper.

Various hydrology factors that form and drive ocean currents as described above have been fully summarized in Table 1. However, both formation and breaking out of water boundary layers, which plays the key role in the causes of turbulence flow, must be added to the Table 1 as the supplement to marine hydrology study, becoming the research gap in future ocean investigation. There is the Figure 1 below to illustrate the water boundary layer theory in my paper.

Table 1. Summary of hydrology forces forming and driving each type of ocean current.

Hydrology elements	The ocean current types applied
Thermal radiation	Warm current; density current
Evaporation	Density current;
Precipitation	Density current;
Cold shrinkage; Convergence and divergence of seawater	Cold and warm current;
Wind stress	Wind drift;
Coriolis force	Geostrophic current;
Gravity forces (Earth, Moon and Sun)	Tidal current;
Uneven density distribution of water	Density current;
Temperature and salinity variation	Thermohaline current;
Inertial force	Inertial current;
The vertical turbulence coefficient	Wind drift;
The geographical latitude of the location	Wind drift;
Friction forces on the seabed or coast	Compensating current;
Friction forces between different water layers	Ekman Drift;
Horizontal pressure gradient caused by various factors	Wind drift;density current;compensating current;
The formation and breaking out of seawater boundary layer	Seawater circulation between surface layer and deeper layer;
River discharge	River discharge current;
The interruption of white waves, beach gaps or low-lying areas, rocky areas on coast	Rip current;
Breaking up in a fractured zone	Longshore current;

My article above has discussed the hydrodynamics of ocean current according to the representative case study of Kuroshio Current. Here it is to further discuss the

formation mechanism of the back flow/counter current in detail on the basis of Figure 1: firstly, along the coast area the current water is imposed by the friction force (F1) generated from the flushing movement between the coast and water, and the water pressure (P1) caused by the friction forces can be efficiently conducted in the same water layer; secondly, the breaking out of water boundary layer near the coast area results in the upwards water flow from bottom layer to surface layer, which leads to the resistance force and pressure (P2) in the surface layer against the flow water of Kuroshio Current. Consequently, both water pressure caused by the friction force and the resistance force imposed by the upwards water flow lead to the back flow/counter current, which becomes the reverse flow core in the middle separating two flow cores of Kuroshio Current described above. Additionally, the upward water flow from deeper layer to surface layer leads to higher water surface level and horizontal pressure gradient, which also causes the force driving back flow. This hydrodynamics is also applicable on the explanation of back flow near the coast of other locations in ocean.

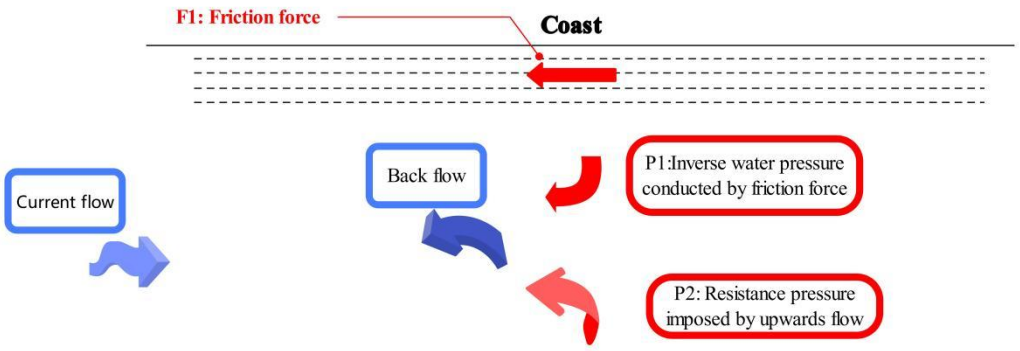

Figure 1a. The hydrodynamics of the back flow/counter current

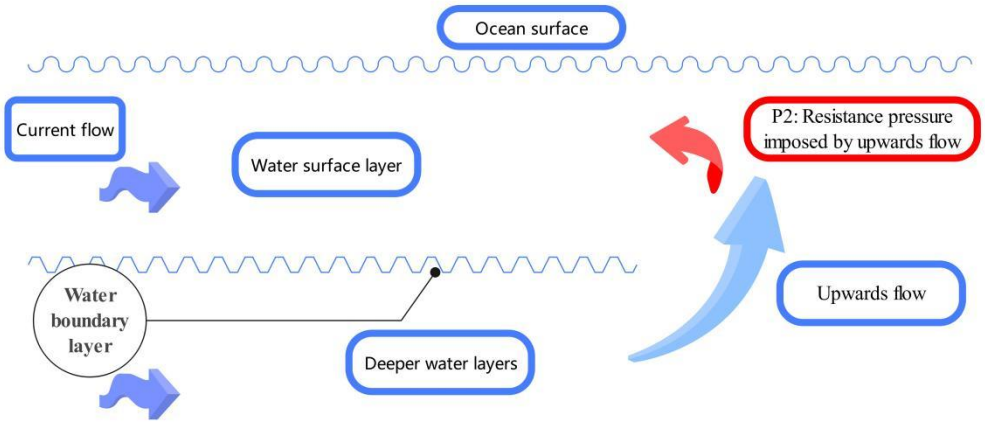

Figure 1b. The upwards flow from deeper water layer to surface layer.

Figure 1. The formation mechanism of the back flow/counter current.

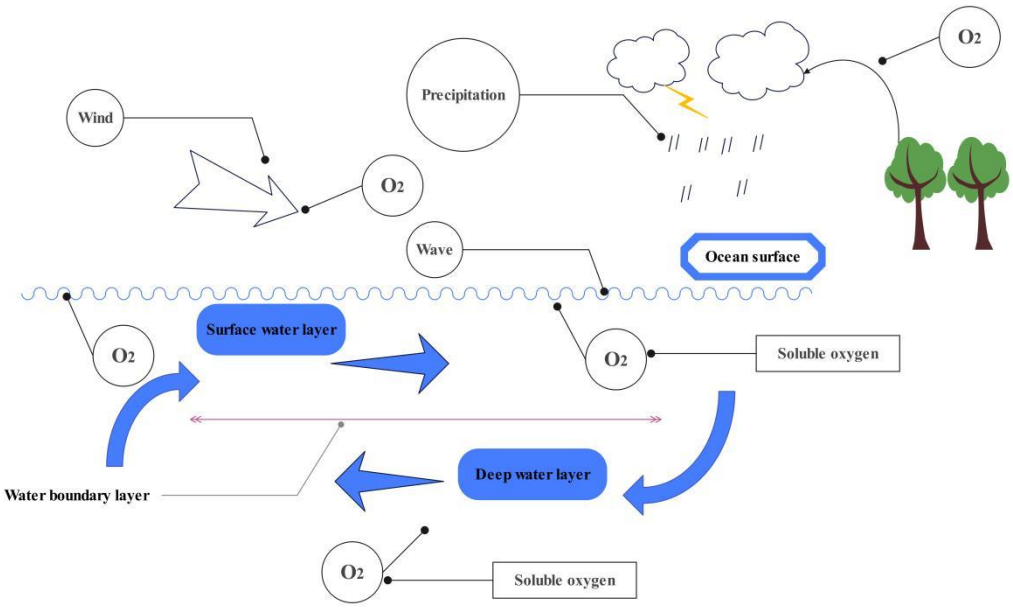

Figure 2. The process of oxygen transport among terrestrial vegetation, atmospheric oxygen and soluble oxygen of ocean.

In Figure 2, the oxygen is firstly produced by the terrestrial vegetation and is then transported in atmosphere [17], which is turned into soluble oxygen of seawater by the mixture effects of wind, precipitation, and waves. The soluble oxygen comes into surface water layer firstly, and then the soluble oxygen is transported into deep water layers by the circulation of seawater between surface water layer and deeper water layers. Consequently, the seawater circulation between different water layers plays the important role in the transport of soluble oxygen into deeper water layers, which is essential for the creatures surviving in the deep ocean.

4.Methods of data collection process

This research project collects the existing data that have been published to re-edit and re-analyze. In the data treatment process, the data used in my article are the estimated data by establishing the regression analysis according to the collected original data, so the data used in my article are the adaptation version, which meet the requirement of 'observational study' project type classified by Open Science Framework. Consequently, the methods obtaining the original data are briefly introduced below:

For the Guan & Hou (2020) research [22], this research utilizes the customer service provided by Remote Sensing Systems (www.remss. com). The interpolated gridded SST data of MW OI is the fusion of observation data from the Microwave Imager (TMI) carried by the Tropical Rainfall Measuring Mission (TRMM) and the Advanced Microwave Scanning Radiometer (AMSR E) carried by the EOS satellite. The sea surface height anomaly data source from the French AVISO (Archiving,

Validation and Interpretation of Satellite Oceanographic Data) program, which integrates multiple satellites, including TOPEX/Poseidon, the height measurement data of ERS-1, ERS-2, etc, and have the spatial resolution of about 25km and the temporal resolution of 1d. The download website for altimeter data is: (http://www.aviso.oceanobs.com/en/data).

For the Cong et al.,(2022) [20] research project, the typhoon wind field data source from NCEP-CFSR (Climate Forecast System Reanalysis) reanalysis data, in combination with the best typhoon path information provided by the Joint Typhoon Warning Center (JT WC), to study the wind field characteristics and changes during typhoons. Changes in water temperature, salinity structure and flow field before and after typhoon passage are all from HYCOM ocean circulation model results （https://www.hycom.org）. The wave data in the sea area is selected from the European Copernicus Marine Environment Monitoring System (CMEMS), deriving the GLOBAL Reanalysis data of REANALYSIS WAV （https://marine.copernicus.eu）.

For Zhou et al., (2017) [25] research project, the field observation data used in this paper are obtained from the onboard CTD observation carried by the 'Science' research ship of the Institute of Oceanography, Chinese Academy of Sciences. The observation station is located in the northeast sea area of Luzon Island, Philippines. CTD observations and water collection are conducted from east to west along the 20° N section, and the temperature and salinity of the water body above 3000m are obtained. The sea surface elevation anomaly (SLA) data is obtained from the official website of the Satellite Oceanography Data Center (AVISO) of the French National Centre for Space Research (ftp.aviso.oceanobs.com). The sea surface current data is obtained by using OSCAR based on satellite, which is calculated as ocean surface velocity inversion of ocean current products (http://www.oscar.noaa.gov). This article uses the five-day average ocean current data provided by it, with a horizontal resolution of 1/3 °. The data of the Oceanography buoy source from the Argo Real Time Data Center in China（http://www.argo.org.cn). The path, intensity, wind speed, and movement speed data of Typhoon Haima are taken from the Typhoon Network of the China Central Meteorological Observatory（http://typhoon.nmc.cn）. The wind field data adopt ERA Interim reanalysis of wind field data provided by the European Centre for Medium Range Weather Forecasts （http://apps.ecmwf.int/datasets/data/interim-full-daily/levtype=sfc/).

Zhu Jing study (2023)[26] mainly utilizes the daily and monthly average data of NCEP/NCAR, CMAP, GODAS, OISST from the National Oceanic and Atmospheric Administration (NOAA) of the United States, as well as the precipitation grid data of CN05.1 in China.

Zhang Li Ping study (2012)[29] adopts the numerical model that is fully coupled by ocean atmosphere model called FOAM (The Fast Ocean-Atmosphere Model）

(Jacob,1997). FOAM is jointly developed by researchers from the University of Wisconsin Madison and Argonne National Laboratory in the United States, and the version used in Zhang li ping study (2012) is FOAM1.5.

5.Wind-driving force: Super Typhoon impact

5.1. Case studies

Studying the changes in marine ecological environment under the impact of typhoon passing through is of significance to systematically understand the response of the ocean ecology to extreme weather conditions, providing essential knowledge for disaster prevention and reduction, as well as for the safety measures during long-distance transportation. On the basis of the Hybrid Coordinate Ocean Model (HYCOM) data, in combination with the Moderate Resolution Imaging Spectroradiometer (MODIS) sensor data carried by the Aqua satellite, the impact of the slowly-moving typhoon ‘Bapeng’ (NO.1929) on several marine indicators was studied, including the sea surface temperature, chlorophyll concentration, vertical temperature and salinity structure, and flow field characteristics of the South China Sea. The observation data were divided into two periods: during the Typhoon ‘Bapeng’ passing through and after Typhoon ‘Bapeng’. The results showed that during the passage of Typhoon ‘Bapeng’, the wave height increased from 3 m to 9 m, while the water flow velocity on the sea surface increased from 0.3 m/s to 0.7 m/s, with the maximum velocity even exceeding 1.8 m/s around the typhoon; After the typhoon passed through, the water temperature on the sea surface dropped from 25.8 ℃ to 24.9 ℃. Under the impact of typhoons, the vertical mixing of water at different depths increased, and the depth of the mixing layer increased by nearly 15 meters, reaching from 23 meters to 38 meters. The upper part of the mixed layer experienced a decrease in temperature and a slight increase in salinity, but the lower part experienced an increase in temperature and a decrease in salinity. The flow velocity at the upper layer of seawater increased with a directional deviation of nearly 90°, but the magnitude of the flow velocity variation gradually decreased from the surface to the bottom. Within 3 days after the typhoon passing through, due to the decrease in temperature and weakened light, the chlorophyll concentration did not rapidly and apparently increase, only showing slight increase on concentration in the short term. This research also deemed that insufficient utilization of nutrients was taken by phytoplankton, although the nutrients was supplemented by vertical mixing enhancement, which consequently did not significantly increase the chlorophyll concentration [20]. However, according to previous research results, it was reported that at one week after the typhoon passed through, the chlorophyll concentration on the surface of the South China Sea began to rapidly increase, which caused primary productivity to significantly improve, bringing additional carbon sink [21].

Guan and Hou (2020) combined multi-source satellite remote sensing observation data and Argo buoy profile observation data to analyze the response of the upper ocean layer of the Northwest Pacific and South China Sea to the super typhoon, Tembin (NO.2012). The results showed that Tembin caused a strong decrease in sea

surface temperature (SST), with the cooling effects mainly concentrated near the typhoon path, and the maximum cooling impact reached 10.3 °C reduction, occurring in the southern sea area of the Korean Peninsula; Another cooler sea area appeared in the eastern sea area of Taiwan Island, with a maximum temperature drop of 5.3 ° C. Microwave and infrared remote sensing of sea surface temperature data had effectively supplemented the shortages of single microwave remote sensing observation in the nearshore area, which observed a large-scale sea surface area influenced by the cooling impact of Tembin near the Korean Peninsula, with the cooling amplitude of more than 5 °C. Based on the fine-grained mixing parameterization method proposed by Gregg et al. (2003), the mixing rate before and after the typhoon was estimated by using vertical high-resolution profiles of both temperature and salinity observed by Argo. It was found that the mixing rate of the upper layer of ocean was significantly enhanced after the typhoon, which was caused by the unstable shearing effect of strong inertial flow induced by the typhoon. Among the three pairs of vertical profiles of temperature-salinity, the mixing rate of two pairs increased by more than 10 times after the typhoon, proving the existence of strong mixing after the typhoon [22].

Super typhoon Tembin caused sea surface cooling at significant and widespread scale in the A3 nearshore area (including East China Sea and Yellow Sea, South Korea Sea in Northwest Pacific). According to Glenn et al.'s (2016) study, the main reasons included:firstly, the vertical temperature gradient in this area during summer of high temperature led it easily to carry more cold water to the surface; Secondly, due to the influence of shallow water topography, the inertial internal waves caused by typhoons in nearshore areas flowed in the opposite direction on the surface, compared with the flow direction at bottom layers, which resulted in vertical shearing effects of flow velocity and induced unstable and strong mixing between surface and bottom layers [23]. Additionally, it was worthwhile noting that in the eastern sea area of Taiwan Island, although the depth of the oceanic background mixing layer was thicker than that of the South China Sea, the cooling amplitude was greater than that of the South China Sea [22], mainly due to the influence of meso-scale cold eddies on the left side of the path before the typhoon passed through, which made the mixing layer shallower so that cold water was easier to be carried from the bottom layer to the surface layer [24].

Zhou et al.,(2017) research analyzed the distribution of marine physics elements in the meso-scale warm vortex located in the northern part of the Luzon Strait during the periods both before and after the Super typhoon ‘Haima’ (2016)’ passage, on the basis of on-site observations of hydrological elements at different water depths near the Luzon Strait, combined with satellite remote sensing data. Its response characteristics to the typhoon was recorded over hydrology observation periods. The results indicated that the warm vortices on the edge of the typhoon were not weakened by the strong cold suction impacts generated by the typhoon's passage; On the contrary, due to the strongly negative vorticity of wind stress anomaly generated at the edge of the

typhoon, the warm seawater at the upper layer of this area spread and sank, with the increase of thickness of the mixed layer, thereby enhancing the warm vortex. The changes in heat energy within the warm vortex before and after the typhoon's passage also confirmed the strengthening of the vortex. In comparison, the warm vortices that were closer to the center of the typhoon were weakened by the cold suction impacts, which was generated by the strongly positive vorticity of wind stress [25].

5.2. Results and Discussion

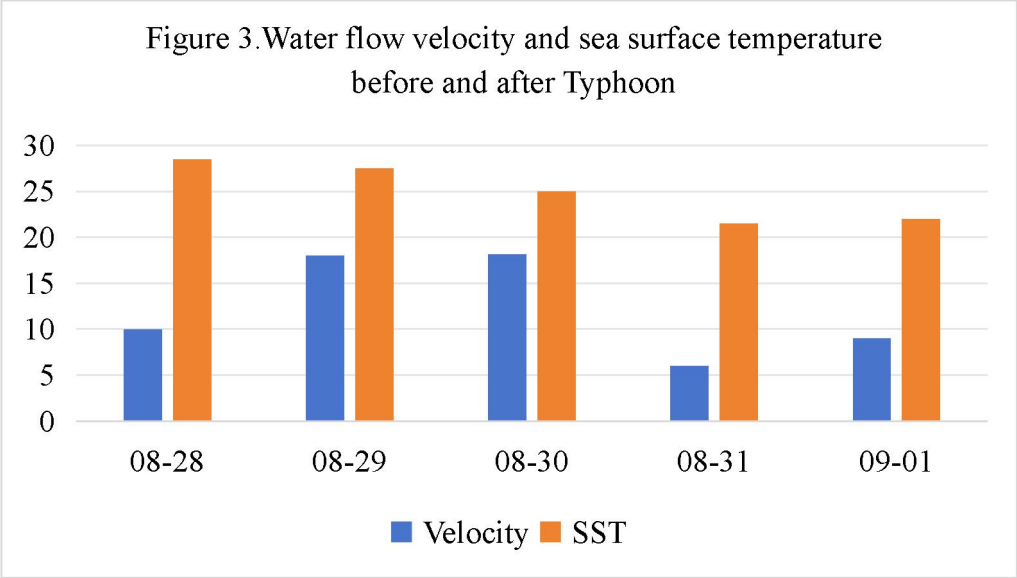

Figure 3. Figure indicates the impact of the super typhoon, Tembin (NO.2012), on both water flow velocity and sea surface temperature. The data are estimated according to the Figure 5 of Guan and Hou (2020) [22].

As could be seen from Figure 3, the super typhoon of Tembin (NO.2012) significantly increased the water flow velocity on August 29th and 30th , when it passed through this sea area, but the surface water temperature did not rapidly decreased correspondingly during these two days. After typhoon passed on August 31th, the water flow velocity decreased to the slowest level, while the surface water temperature descended to the lowest level at the same day, indicating that there was a lag period of cooling effects caused by typhoon. Guan and Hou (2020) proposed that this cooling effects was mainly due to the mixing and entrainment of the ocean water caused by the strong winds of the typhoon itself [22]. Nevertheless, my article disagreed with this explanation, because the lag period of cooling effects pointed out in Figure 3 revealed that the descending of surface water temperature was not directly attributed to the mixing and cold suction impacts generated by the typhoon's passage itself. The upward meso-scale flow from the colder and deeper water layers to the surface water layer should be the main reason to explain this lag period of cooling effects caused by typhoon, because the meso-scale circulation from the colder and deeper water layers to the surface water layer obviously took longer time to decrease the surface water temperature. The water boundary layer between surface water layer and deeper water layer was destroyed by the strong wind disturbance of typhoon, resulting in the

upward flow from the colder and deeper water layers to the surface water layer, so that the surface water temperature was decreased by the mixture effect, which was further illustrated in Figure 6 below.

As the supplement to Cong et al.,(2022) research [20], Figure 4 further illustrated the hydrology characteristics at different seawater depths under super typhoon disturbance. From the Figure 4a, the surface water temperature apparently decreased at the shallow water depth of 10m, whereas the seawater temperature even slightly increased at water depth of 50m after typhoon passed through, and there was no significantly difference in water temperature at deeper water depths (100m~1500m); For the water flow velocity shown in Figure 4b, the typhoon caused the flow velocity significantly to increase at shallow water depth of 10m only, but there was no significantly variation in water flow velocity at deeper water depths; However, the water flow direction was more complicated at deeper water depths: as seen from Figure 4c, before the typhoon coming, the water flow directions at depths from 10m to 500m was not consistent with the flow direction at depths of 1000m, and this inconsistency of flow direction between upper seawater layers and bottom layer should be attributed to the driving force of Geostrophic current, which was discussed in detail at above sections of my article. After typhoon passed, the water flow direction was apparently altered at deep water depths of 1000m, which might indicate the strong evidence of the upward meso-scale circulation from the colder and deeper water layers to the surface water layer, due to the destruction of water boundary layer by typhoon as discussed in Figure 3 of my article.

Figure 4a. Temperature Variation at different water depths before and after Typhoon

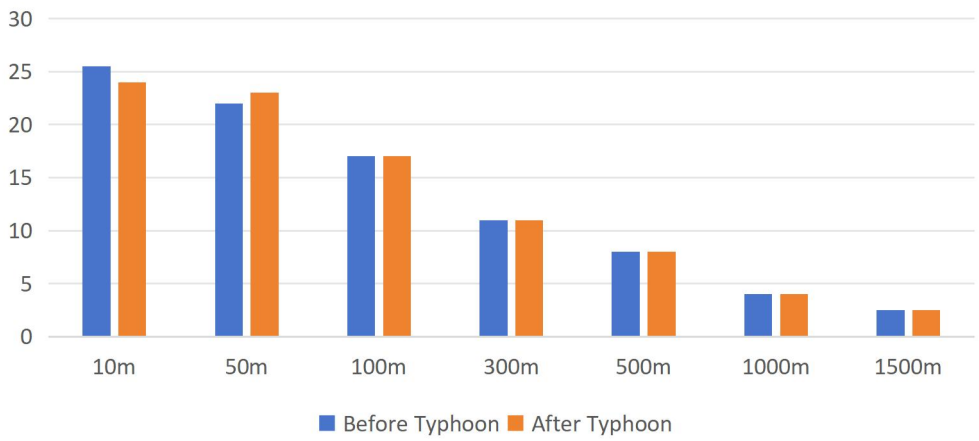

Figure 4b. Water flow velocity at different depths before and after Typhoon

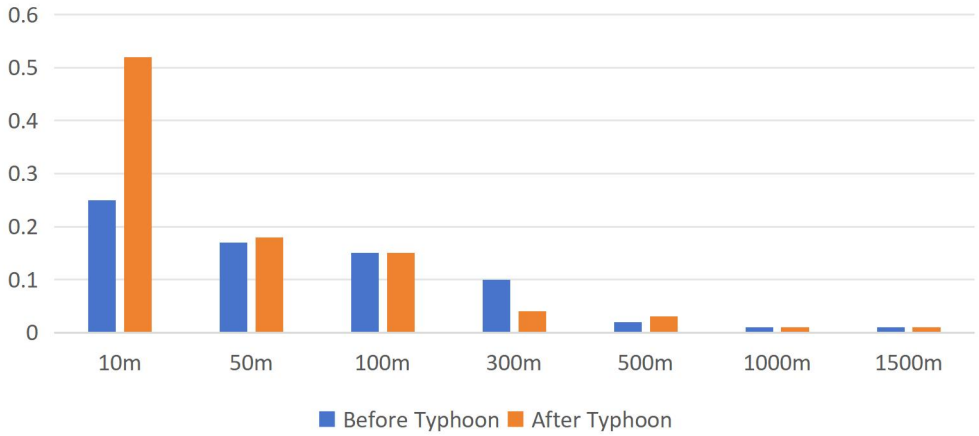

Figure 4c. Water flow direction at different depths before and after Typhoon

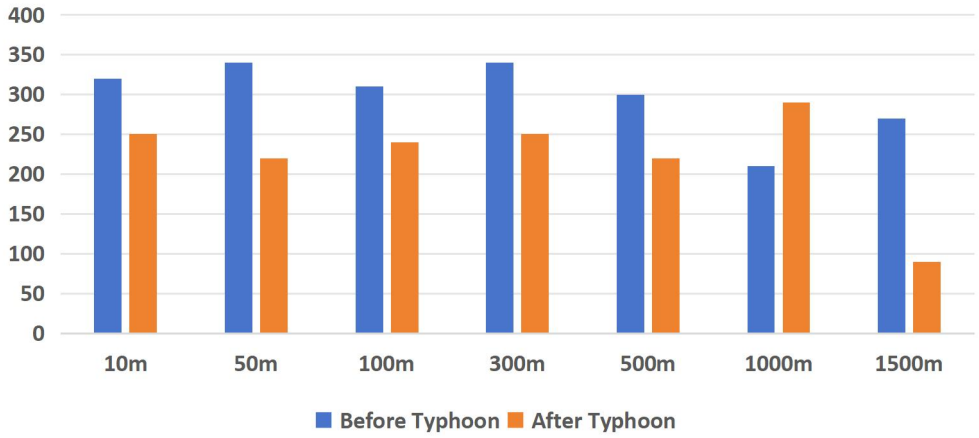

Figure 4. This figure indicates the impacts of Typhoon 'Bapeng' (NO.1929) on the water temperature, water flow velocity and water flow direction at different water depths. The data are estimated according to the figure 6 of Cong et al.,(2022) [20].

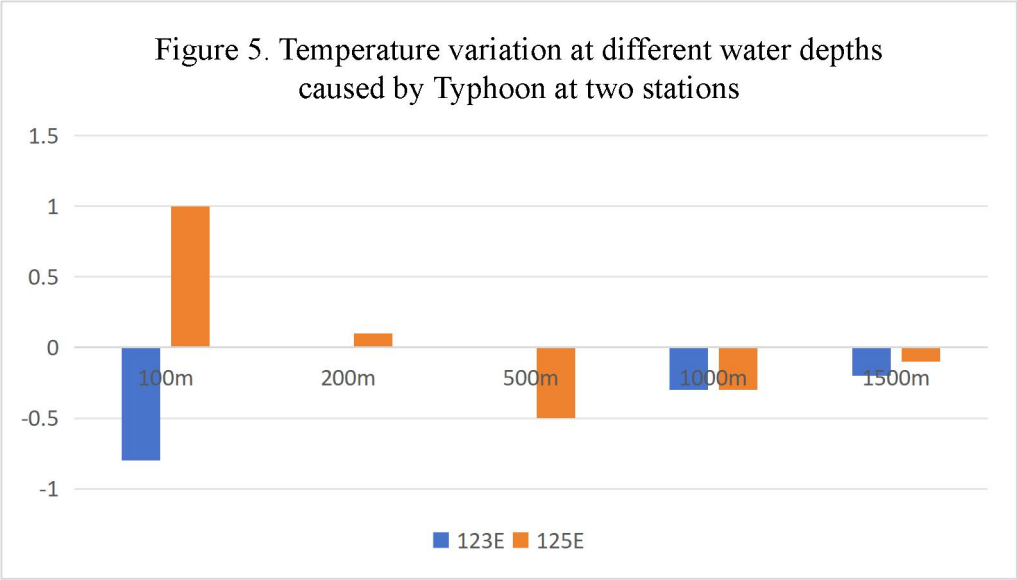

Figure 5. This figure indicates the impacts of Super typhoon 'Haima' (2016) on water temperature at different water depths observed by two representative stations. The data are estimated according to the Figure 5 of Zhou et al., (2017) [25].

Figure 5 compared the temperature variations at two representative stations: station 123E, which was nearby the typhoon centre, observed the decreased water temperature caused by typhoon, whereas the water temperature at station 125E, which was away from the typhoon centre (at the edge of typhoon), significantly increased after typhoon passed through. As the supplement to the Zhou et al., (2017) research [25], my article applied the new water boundary theories to further analyze this natural science discovery: firstly, in the seawater area nearby the typhoon centre, the water boundary was easily broken up by the strong disturbance of typhoon, so upward water flow was formed from the colder and deeper water layers to surface water layers, which reduced the SST as discussed above; secondly, in the meso-scale warm vortex away from the typhoon centre observed at station 125E, the water boundary layer between surface layer and deep layer was still stable, but this boundary layer sank into deeper depths because the seawater at deep layers of station 125E flowed into the seawater area nearby the typhoon centre, forming the compensation current to the upward seawater flow nearby the typhoon centre; Thirdly, the previous warm seawater nearby the typhoon centre before typhoon flowed into the meso-scale warm vortex located at station 125E to increase the SST, which formed the meso-scale water circulation. The above three causing factors have been described in Figure 6. Consequently, the meso-scale water circulation between upper layer and deeper layers caused the temperature variations observed at two representative stations in Figure 5. The concentration and sinking of warm seawater from the sea area nearby the typhoon to the warm vortex located at station 125E significantly increased the heat energy at this station, which was consistent with the heat observation data. Additionally, the slightly increased seawater temperature at water depth of 50m after typhoon passed

through, which was shown in Figure 4a, would also indicate the boundary layer sinking effect.

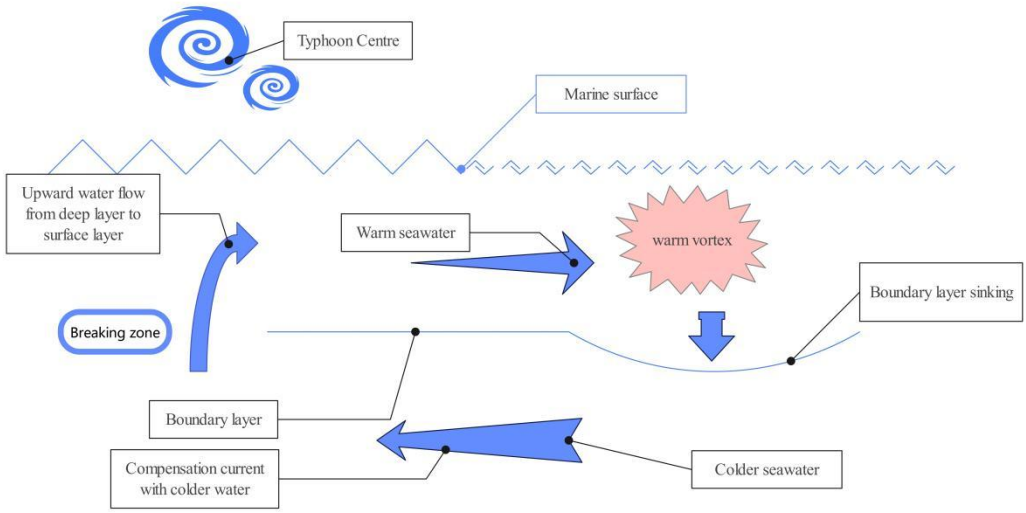

Figure 6. The meso-scale seawater circulation between upper layer and deeper layer in the marine area influenced by super typhoon.

6.Sea-Air interaction

6.1.Case study

The anomalous changes in sea surface temperature of the Maritime Continent (MC) are deemed to closely relate with climate anomalies in the Asia Australia region. This research has mainly collected the daily and monthly average data of NCEP/NCAR, CMAP, GODAS, OISST from the National Oceanic and Atmospheric Administration (NOAA) of the United States, in combination with the precipitation grid data of CN05.1 in China, to systematically study the characteristics of sea surface temperature anomalies in the oceanic continental (MC) region of the Northern Hemisphere during summer (from June to August). The temperature changes after sequentially filtering out ENSO（El Niño-Southern Oscillation) signals and IOD (Indian Ocean Dipole) signals, the occurrence characteristics and causes of ocean heat wave events in the region have also been identified to analyze the impact of sea surface temperature anomalies on climate anomalies in Asia and Australia [26].

It was found that different patterns of sea surface temperature variation in oceanic continental regions led to different impacts on precipitation in the Asia-Australia region through sea-air interactions. The main findings included: firstly, the sea surface temperature anomalies in the oceanic continental regions of the Northern Hemisphere during summer were tightly related to the summer climate anomalies in East Asia. There were two indicators of synergistic changes, including Sea Surface Temperature Anomaly (SSTA) of in summer oceanic continental regions and Sea Level Pressure Anomaly (SLPA) in East Asia, which were analyzed by using methods such as

Singular Value Decomposition (SVD). The first two modal characteristics and climatic effects of this synergistic variation were investigated by this research. [26].

The results indicated that the sea surface temperature anomaly in the MC region of SVD1 (the first mode of SVD analysis) displayed as an temperature anomaly of warm sea surface over the entire region, while the pressure anomaly of sea surface in East Asia was the positively correlated anomaly over the entire region. In comparison to the SVD1, the temperature anomaly of sea surface in the MC region of SVD2 (the second mode of SVD analysis) was different, reversed from east to west with warm anomalies in the east and cold anomalies in the west respectively, while the sea surface pressure anomaly in East Asia was reversed from north to south, with positively correlated anomalies in the north and negatively correlated anomalies in the south, respectively. It was deduced that the formation of sea surface temperature anomalies in two modes was determined by both ocean dynamics and changes in heat flux. The anomalous mode of sea surface pressure in East Asia was deemed as an anomalous anticyclone in the northwest Pacific in SVD1, while in SVD2 it was considered as a circulation anomaly that was similar to PJ/EAP over the western Pacific. Under the influence of different circulation configurations, when PC1 (the time series of SVD1) was during the positive phase, the precipitation in the middle and lower reaches of the Yangtze River in China and in the southern side of the the Yunnan-Guizhou Plateau was concurrently positively correlated, but the precipitation in both central and northeastern China was negatively correlated. When PC2 (the time series of SVD2) was under the positive phase, most areas of the middle and lower reaches of the Yangtze River, the Hetao region and the southwest region of China was manifested as positively correlated precipitation anomalies, whereas the Huaibei and Northeast regions showed negatively correlated precipitation anomalies. It was found that the sea surface temperature anomalies in oceanic continental regions were mainly related to the factors of local variability, ENSO and IOD, so the main patterns of summer sea surface temperature anomalies in oceanic continents and their relationship with climate anomalies were further explored by the empirical orthogonal function (EOF) analysis. After filtering the ENSO signal, the first mode of summer oceanic continental SST anomaly became a uni-polar SST anomaly distribution, with significantly inter-annual variation [26].

The maintenance mechanism of sea surface temperature anomalies was independent of ENSO, which varied in different regions of oceanic continents, especially in southern Java and in the tropical northwest Pacific. When PC1 was in the positive phase, there was the warm sea surface temperature anomaly in the southern region of Java Island, which was maintained by ocean dynamic heating system in the area. Affected by Gill's response, there had been an abnormal upward movement of the atmosphere in the region. In the tropical northwest Pacific region, the mode of non adiabatic cooling in the atmosphere dominated, as there was less cloud cover and the warm sea surface temperature anomalies was maintained by absorbing shortwave

radiation. The caused tilted vertical circulation connected the tropical southeast Indian Ocean with the tropical northwest Pacific Ocean, while the anomalous circulation in the Asia-Australia monsoon region was influenced by this sea surface temperature anomaly mode that was independent of ENSO signals, which resulted in an abnormal decrease in summer precipitation at the southeastern coastal areas of China but caused an abnormal increase in winter precipitation outside the tropical regions of Australia, respectively. After filtering out both ENSO signals and IOD signals, the main mode of sea surface temperature anomalies in summer oceanic continental regions remained as the uni-polar warm sea surface temperature anomaly. Under the positive phase of PC1, the area with the highest value of warm sea surface temperature anomaly was located at the western waters of New Guinea Island, mainly consisting of decadal components with a period of about 11 years. The average sea surface temperature anomaly index (IFEI) in the MC region had been defined to be highly correlated with the EOF1 mode. In comparison, under the positive phase for time coefficient of IFEI, the dominant factors maintaining the anomalous sea temperature in different regions of the MC area were different. The northeastern sea area of MC was mainly affected by the meridional advection term and shortwave radiation anomalies in the oceanic subsurface, whereas in the Bay of Bengal and the western sea area of New Guinea, shortwave and longwave radiation anomalies were the main contributing factors to sea surface temperature warming. The sea surface temperature anomaly further affected the circulation anomaly, showing that the abnormal non adiabatic heating of the atmosphere, at the location near the Java Island and in the equatorial region east of New Guinea Island, forced the atmosphere to produce easterly anomalies near the equator, which formed significant anomalous anticyclonic circulation in the northwest Pacific region. Affected by the abnormal circulation field, the precipitation significantly increased in the southwest of the MC region and in southern China, but the precipitation in the northwest Pacific region decreased, especially near the Philippine Islands [26].

It was reported that the continuous occurrence of Marine Heatwave (MHW) events in the MC region during summer was mainly influenced by the abnormal warming of sea surface temperature in summer, which included both the impact of local sea surface temperature warming caused by global warming and the influence of inter-annual sea surface temperature modes generated by the sea-air interactions. The amplitude of the heatwave events duration was increasing with global warming at oceanic continental regions. The main pattern of abnormal periods for the ocean heatwave events did not only show a long-term trend, but also exhibited significant inter-annual characteristics. After filtering out inter-decadal signals, the total number of days for the ocean heatwave events at north of the equator increased abnormally under the positive phase of PC1, with the highest values located in the South China Sea and in the western Pacific region north of New Guinea. The abnormal ocean currents in the seawater near Java Island had led to the accumulation of warm seawater, which was beneficial for the rise of sea surface temperature in the region, resulting in a single prolonged event of ocean heat wave. In the northwest Pacific, the

ocean warmed up due to receiving more heat flux, which was conducive to the continuous occurrence of ocean heat waves. Under this mode, the precipitation in the northeastern part of the oceanic continent decreased, but increased in the southwestern part and the southeastern part of China, as well as in the North China Plain and in the Korean Peninsula. These results were beneficial for better understanding on the characteristics of sea surface temperature anomalies in oceanic continental regions and their relationship with climate anomalies in Asia and Australia, which provided scientific evidence for further research on climate anomalies in Asia and Australia [26].

According to the observation data and modeling technology, it is indicated that the seawater circulation is strengthening under the background of global warming. The variation in the seawater circulation can affect the freshwater flux in the ocean, inducing anomalies in ocean salinity, flowing field and temperature field, while the anomalies in the ocean can further interact with the atmosphere, thereby triggering global climate adjustments. For example, changes in the seawater circulation can also affect the water vapor content and non-adiabatic heating rate in the atmosphere. Water vapor in the atmosphere is one of the most important greenhouse gases, whose impact is the most significant factor causing the process of global warming. The phase transition process of water vapor leads to abnormal latent heat flux, which ultimately affects the polar heat transport in the climate system [29].

This research project focused on the impact of seawater cycle variation on ocean circulation and climate. According to the Fast Ocean Atmosphere Model (FOAM1.5), observation and re-analysis of data, as well as the model results from the Intergovernmental Panel on Climate Change (IPCC), the research systematically studied the important role of ocean freshwater flux and water vapor, which was induced by water cycle changes in the climate system. The observation and analysis of the past 30 years further indicated that changes in the water cycle resulted in significantly regional dependencies. A typical feature was that the Evaporation Minus Precipitation (EmP) of the global western boundary current and its extension areas was greater than zero, especially in the Kuroshio Current, Gulf Stream and their extension areas, which meant that there was a net loss of freshwater in the western boundary flow and its extension area. This research also adopted the approach of speculating from the small scale, firstly focusing on the sea area with the largest abnormal freshwater flux, namely the Kuroshio pro tidal, Gulf Stream and its extension areas, which was based on a coupled ocean atmosphere model of FOAM to explore the climate effect of freshwater loss caused by the Kuroshio Current, Gulf Stream and their extensions. The model results indicated that the net loss of freshwater in the Kuroshio Extension (KOE) region had generated the anomaly in cyclonic circulation spanning both the subtropical and subarctic regions, which induced anomalous cold advection southward on the western side of the North Pacific but resulted in anomalous warm advection northward on the eastern side of the North Pacific. The abnormal temperature advection ultimately generated seawater surface

temperature (SST) dipoles at the mid latitude, in terms of cold SST in the west and warm SST in the winter. The response of the North Pacific atmospheric circulation to freshwater flux in the KOE region was characterized by a quasi anomaly of both positive pressure and low pressure, which was mainly related to the warm anomaly of the equatorial western Pacific SST, whereas the local SST changes in the North Pacific played a suppressive role in the anomaly in freshwater flux pressure, and the freshwater loss in the KOE region had strengthened both the latitudinal SST gradient at the equator and the El Ni ñ o Southern Oscillation (ENSO). This anomaly was the result of multiple mechanisms working together, including the coupled mechanism of surface wind- evaporation-SST (WES), the sub-duction process of equatorial warming anomalies, and the acceleration of density-driven overturning flows at deep radial direction. The freshwater loss in the Gulf Stream and its extended regions also forced abnormal cyclonic circulation with dipole structures of SST, but the dipole of SST exhibited a northeast southwest tilt rather than an east-west distribution again, which was related to the distribution of land and sea in the Atlantic Ocean. The response of the North Atlantic atmospheric circulation showed significant seasonality, manifested as a low-pressure anomaly similar to the negative phase of the North Atlantic Oscillation (NAO) in early winter, and a high-pressure anomaly similar to the East Atlantic Mode (EAM) in late winter, respectively. The net loss of freshwater in the Gulf Stream and its extended regions simultaneously strengthened the flow of Atlantic Ocean radial overturning current (AMOC) and the heat transport of northward polar, ultimately leading to temperature anomalies at the equator. The loss of freshwater in the Gulf Stream and its extended region caused the response similar to El Ni ñ o warming in the equatorial Pacific but the cooling response in the North Pacific. The warming of the equatorial Pacific enhanced the atmospheric response of the North Atlantic in early winter by stimulating Rossby waves, but subsequently resulted in the suppressive effect in the late winter. Overall, the air-sea coupling process in the equatorial Pacific suppressed the response of the North Atlantic ocean and atmosphere, whereas the local air-sea coupling process in the North Atlantic played a promoting role [29].

After exploring the climate effects of freshwater flux anomalies on marine areas (KOE, Gulf Stream and its extended regions), which was induced by seawater circulation, research focus was turned to be the global stage. The FOAM model was adopted to simulate global warming (under CO_2 concentration doubling conditions), based on which it was to evaluate the role of ocean freshwater flux variation induced by the water cycle in global warming. The simulation results indicated that global warming had led to the strengthening of circulation, resulting in the desalination at both low latitude and high latitude sea area, but the salinity of mid latitude and subtropical seawater was increased. It was found that strengthening the water cycle could amplify global warming. At the global scale, this amplification effect was mainly related to the desalination of high latitude seawater. The weakening of high latitude seawater salinity could lead to the shallower average depth of the mixing layer globally, which weakened vertical mixing, and ultimately more CO_2 induced

warming was accumulated in the ocean surface. The modulation effect of freshwater flux changes on the latitudinal distribution of SST was very complex. In the Northern Hemisphere, the weakening of high latitude seawater did not only concentrate more CO_2 induced warming on the ocean surface, but also weakened the intensity of radial overturning currents, resulting in more warm water accumulating on the sub surface of the ocean. The latitudinal difference in sea surface salinity led to convergence of the mid latitude flow field, thereby amplifying the warming in mid latitudes and weakening the warming in the sub-polar sea area. In the southern hemisphere, the warming of SST caused by the weakening of high latitudes triggered anomalous winds easterly through local air-sea coupling processes, thereby inducing polar Ekman warm advection in mid latitudes. The anomalous Ekman warm advection greatly counteracted the salinity-induced northward cold advection, which was similar to the cold anomaly at high latitudes in the Northern Hemisphere, thereby maintaining the warm anomaly at mid to high latitudes in the Southern Hemisphere [29].

In addition, atmospheric feedback processes that were related to global warming had also contributed to the warming of SST, which could be revealed by the atmospheric water vapor changes. Based on the long-term reanalysis data of 20CRv2, it was found that the time series of annual average water vapor mainly had three types of temporal scale variation: long-term trend, inter-annual variation, and decadal variation. The long-term trend of water vapor was closely related to global warming, and the inter-annual and decadal variations of water vapor were associated with the fluctuations of natural variability in ENSO and AMOC, respectively. The synchronous changes of water vapor and SST on the global scale was attributed to the simple thermodynamic Clausius Clapeyron (C-C) theory under constant relative humidity conditions. At the regional scale, the integrated water vapor balance of the entire atmosphere indicated that the spatial structure of water vapor, which was related to global warming, AMO and ENSO, should be largely attributed to the mean circulation dynamics, especially including the large-scale convergence divergence circulation induced by SST. From middle to high latitudes, transient vorticity and thermodynamics also played a very important role [29].

6.2. Results and Discussion

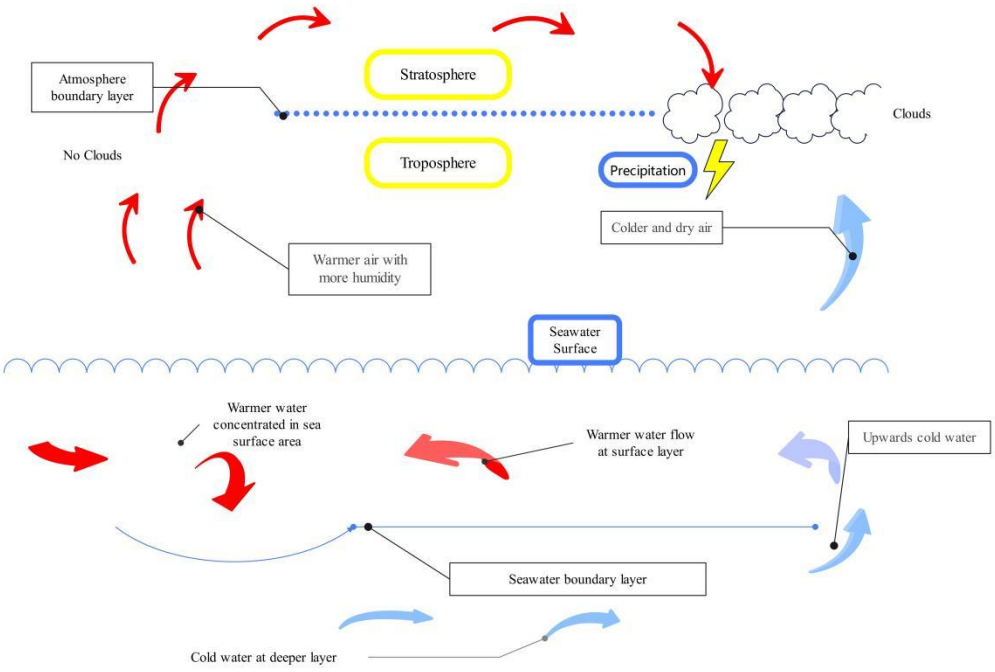

Figure 7. The conceptional model of interaction between seawater circulation and air circulation.

After this case study, my article has designed a conceptional model in Figure 7 to illustrate the interaction between seawater circulation and atmosphere circulation, which demonstrates the effects of sea water temperature variation on the climate: firstly, the colder water at deeper seawater layer flows into the breaking up zone of seawater boundary layer, forming the upwards colder water flow, while the adjacent warmer seawater flows and concentrates at another sea surface area, so that the seawater circulation between the sea surface layer and deeper seawater layer is formed at meso-scale, as discussed in detail above. In the warmer sea surface area, the warmer air with higher humidity goes up efficiently from troposphere to the stratosphere, due to the absence in clouds. However, in the colder sea surface area, the colder and dry air is clustered under the clouds, staying in the troposphere. When the warmer air with higher humidity, which rises from the warmer sea surface area to the stratosphere, transports in a parallel route along the atmosphere boundary and subsequently arrives in the colder and cloudy atmosphere area, the precipitation is formed due to the condensation effects. Figure 7 is also the example illustrating the new atmospheric boundary theory proposed by my another article [27]. By comparison and contrast, the atmosphere convection during precipitation event in Figure 7 is that the warmer air goes down while cold air goes up, which occurs at higher height between troposphere and stratosphere; in the Figure 1 of my another article [27], the convection mode of urban heat island is opposite: the warmer air rises while colder air drops down, which occurs at lower height (in the troposphere only).

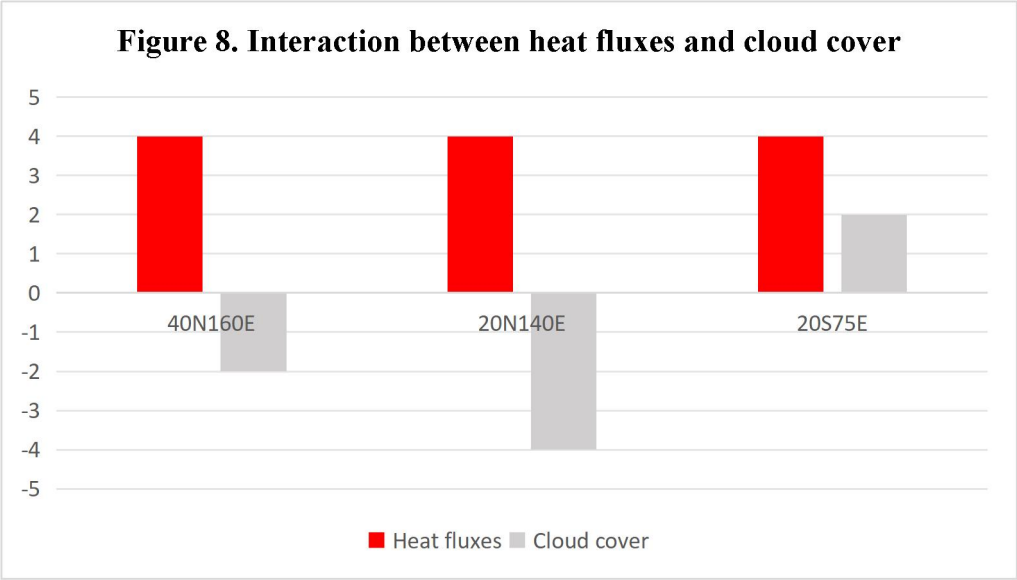

Figure 8. Figure 8 indicates the interaction between sensible heat net fluxes anomalies (W/m^2) and total cloud cover anomalies (%) at different locations. The data is estimated according to the figure 5 of Zhu jing (2023)[26].

As shown in Figure 8, at locations of both 40°N160°E and 20°N140°E, the sensible heat net fluxes is 4 W/m^2, while the clouds cover is -2% and -4% respectively, indicating less cloud coverage in these two locations with 'hot spot' temperature anomalies. In comparison, the 'hot spot' at location 20°S75°E shows more cloud coverage of +2%, revealing the different mode of heating fluxes from the first two locations. According to the Zhu Jing (2023) records, the hot temperature at the first two locations is positively correlated with the precipitations in the areas of the southwestern part and the southeastern part of China. Consequently, the air circulation pattern can be deduced on the basis of the my conceptional model of Figure 7: the warmer air with moisture ascends from the sea surface into the stratosphere efficiently due to the absence in clouds cover at the first two locations of 'hot spot'; then the air transports in a parallel route along the atmosphere boundary and subsequently arrives in the southwestern part and the southeastern part of China; when the warmer air with moisture from the ocean meets the clouds with colder and dry air in the continent, precipitation occurs.

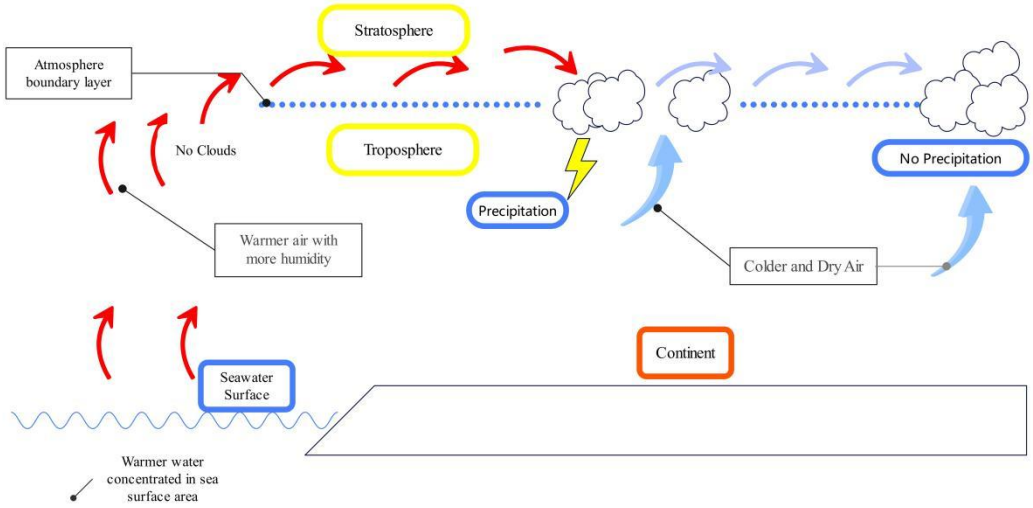

Figure 9. Figure 9 indicates the sea-air interaction: the hot spot of sea surface area at the left of figure is positively correlated with precipitation events in the middle of continent, and is negatively correlated with precipitation events on the right of continent in figure.

Figure 9 further demonstrates the sea-air interaction and explains the correlations between the 'hot spot' occurrence of sea area and the precipitation events in the continent: the warmer air with moisture ascends from the sea surface into the stratosphere efficiently due to the absence in clouds cover at the 'hot spot' on the left of figure; then the air transports in a parallel route along the atmosphere boundary and subsequently arrives in the middle of continent; when the warmer air with moisture from the ocean meets the clouds with colder and dry air in the middle of continent, precipitation occurs. Consequently, the 'hot spot' occurrence of the sea is positively correlated with precipitation event in the middle of continent, where the vertical air convection mode is that the colder and dry air goes up while the warmer and precipitation drops down. Subsequently, the colder and dry air continues to transport in a parallel route along the atmosphere boundary and finally clusters at the right of continent in the figure, which does not meet the conditions of precipitation occurrence, so the precipitation occurrence at the right of continent in the figure is negatively correlated with the 'hot spot'. This new demonstration process would be the conception model explaining the correlation results between the warm sea surface water and the precipitation events in the continent, as reported in Zhu Jing (2023) study [26]. Further more, the atmosphere circulation shown in Figure 9 should become the representative case illustrating the compensation mechanism of precipitation among different locations with various meteorological conditions: when the precipitation event occurs in one location, another location may face drought stress due to the colder and dryer air circulation on two sides of boundary layer.

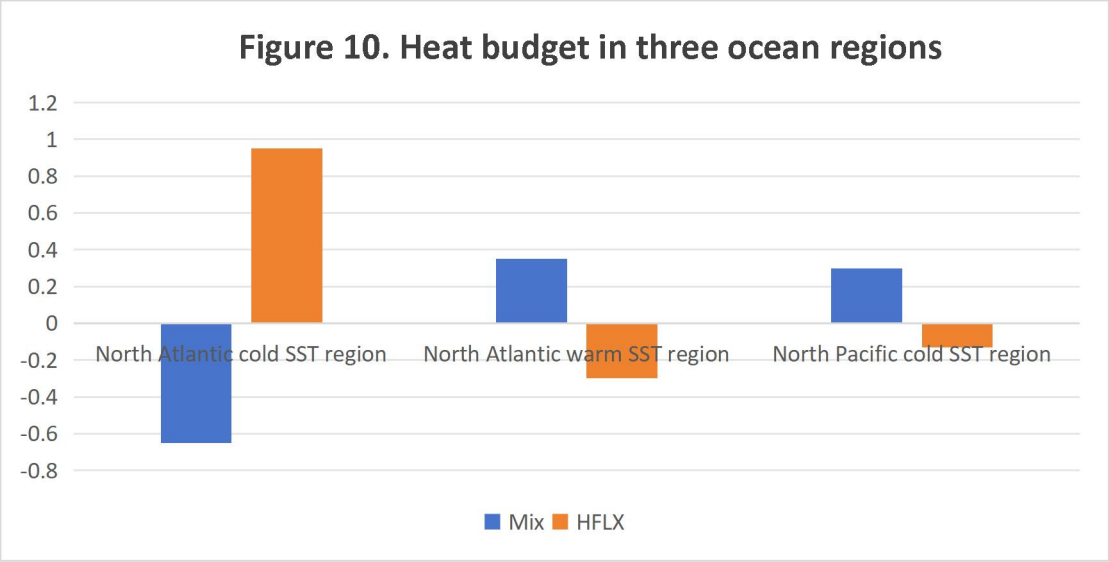

Figure 10. Heat budget in three representative ocean regions. HFLX, Mix are the surface net heat flux (positive –downward, scaled by 1/(ρ Cph)) and mixing heat respectively, and the units for temperature and heat budget term are defined as °C and $5*10^{-8}$ °C /s, respectively. The data is estimated according to the Figure 4.5 of Zhang li ping study(2012)[29].

As can been seen from Figure 10, the surface net heat flux was positive influx at approximately 0.95 but the heat flux at mixing layer was negatively efflux at around -0.65 in North Atlantic cold SST region; in comparison, at locations of both North Atlantic warm SST region and North Pacific cold SST region, the surface net heat flux turned to be negatively flowing out, whereas the heat flux at the mixing layer became positive influx. However, the negative flowing out of HFLX in North Pacific cold SST region was apparently less than it in North Atlantic warm SST region. Zhang li ping study (2012) explained these results as [29]: The southward flow induced by cyclonic circulation anomalies brought cold water from high latitudes to low latitudes, resulting in the cold anomaly southwest oriented. On the other hand, the abnormal northward flow took warm water from the subtropical zone to high latitudes, leading to the generation of warm anomalies in the northeast direction. In both regions, the abnormal salinity had strengthened vertical mixing. In the sub-polar sea area of the North Atlantic, vertical mixing strengthened the movement of cold water from surface layer to the lower ocean layer, thereby contributing to the warming of the sea surface temperature (SST) in this area. On the other hand, in the southwest corner of the subtropical zone, strong mixing brought cold water from the subsurface to the surface, increasing the cooling of SST.

Nevertheless, my article proposes new discussion with regards to the SST anomaly, which is demonstrated more specifically in each location: in the North Atlantic cold SST region, the positive surface net heat flux reveals that more warmer water is transferred into this area from other ocean areas through the upper surface layer, becoming the compensation current at the upper surface layer. Although the negative

heat flux at the vertical mixing layer indicates some heat efflux at the deeper layer, the heat influx from the warmer current at upper layer is more than the heat efflux at the mixing layer. However, there are two source streams of warmer compensation current causing the warming in North Atlantic cold SST region: one stream is from Carribean located at the Southwest, and the other stream is water circulation from the North Atlantic warm SST region located at the Northeast, which can be proven by the Figure 3-17 of Zhang li ping study (2012)[29]; In the locations of both North Atlantic warm SST region and North Pacific cold SST region, the positive heat flux in the vertical mixing layer would indicate the warmer surface water transferring from the upper surface layer to the lower ocean layer, because the water temperature should be obviously warmer at the upper surface layer than it at the lower ocean layer in the North Atlantic warm SST region, resulting in the efflux of net surface heat flux from surface layer into lower layer. However, the positive heat flux at the mixing layer of North Atlantic warm SST region is more than it at the mixing layer of North Pacific cold SST region, therefore leading to more efflux of surface net heat flux in the North Atlantic warm SST region, and this explained consequence of heat flux direction is more consistent with the observation data in Figure 10.

7. Current circulation at the upper layer of seawater

7.1. Case study

The analysis showed that the seawater circulation at the upper level exhibited significantly seasonal variations influenced by the Indian monsoon in the studied sea area. Both the equator ocean and the South China Sea displayed periodic variations in three flowing streams, including the Wyrtki jet stream, the Southern Equatorial Current, as well as latitudinal movements of the Southern Equatorial Current. There was the seasonal reversal direction of large-scale circulation at the north of the equator found: during the southwest monsoon period, three streams of ocean currents, including the southeast-oriented West India coastal current, the eastward southwest monsoon drift and the northward East India coastal current, together formed an anticyclonic circulation, but its circulation direction was basically reversed during the Northeast monsoon period. In sync with this circulation reversion, the ocean currents in the eastern part of the Bay of Bengal mainly flowed in south direction during the southwest monsoon period, and changed into north direction during northeast monsoon period, while the flowing direction at the western part of the bay mouth was generally the opposite to the eastern part. This variation in circulation structure caused that external ocean water could enter the bay through the west side of the bay mouth during the southwest monsoon period, while the water in the bay was likely to enter the equatorial Indian Ocean via the east side of the bay mouth, but this water exchange pathway turned to be opposite during the northeast monsoon period [28].

The analysis of water mass showed that the water in the Bay of Bengal was mainly distributed in the Arabian Sea, offshore Sumatra Island and equatorial oceans outside the bay, whose distribution range varied seasonally: from November to March of the following year, the water mass in the Bay of Bengal was mainly distributed in the

southeastern Arabian Sea, and appeared in the offshore and equatorial waters of Sumatra Island from June to October, lasting until February of the following year; The distribution range of Arabian seawater in the equatorial sea area manifested semi-annual variation, which extended eastwards along the equator from May to June and from October to January of the following year, reaching the sea area at east of 90°E. In addition, during most months (from June to April of the following year), Arabian seawater still stayed in the bay. The seasonal variation in the distribution of two water masses was mainly determined by the upper level circulation. From November to March of the following year, there were two main flowing paths from the Bay of Bengal transported into the southeastern Arabian Sea, including the East India coastal current southward along the western boundary of the Bay of Bengal and the coast of Sri Lanka, as well as the southwest northeast monsoon drift. From June to October, the water mass from the Bay of Bengal was continuously transported southward into the equatorial sea area via the eastern side of the bay mouth, and then flowed into the seawater off Sumatra Island, even entering the equatorial sea area. The semi-annual fluctuations in the distribution range of Arabian seawater in equatorial sea area were related to the Wyrtki jet stream in spring and autumn, which formed two paths for the Arabian seawater invading into the bay: from November to April of the following year, it flowed continuously northward and entered the bay from the equator through the east side of the bay mouth, while from June to September, Arabian seawater was transported to the bay by southwest monsoon drift. The hydrological survey data during the transition period of Southwest Monsoon in 2011 also showed similar transport characteristics between the two water masses. The calculation results of net salt flux indicated that the salt exchange process inside and outside the Bay of Bengal was mainly driven by ocean currents, but the processes were basically opposite between the east and west sides of the bay mouth. During the southwest monsoon period, the net salt flux to the north was found to be on the west side, and the net salt flux to the south was on the east side. During the northeast monsoon period, the net salt flux to the south was located on the west side, while the net salt flux to the north was reported on the east side. Based on the freshwater transport formula, it was calculated that the average annual output of freshwater from the 6°N section of the Bay of Bengal was 0.1Sv [28].

7.2. Discussion

In summary, the seawater circulation can be formed between upper and lower ocean layers, or driven at the upper surface ocean layer only, both of which have been studied in detail above. These two modes of seawater circulation together play the significant role in the pollutant transport in the ocean, which is discussed next.

8. Pollution in ocean water

8.1. Case studies

So far, research on the migration and transformation of ocean pollutants at both domestic and international scales has been limited to individual study of single pollutant species, without systematic summary, most of which are qualitative

descriptions lacking of quantitative calculations. The main pollutant species in Xiamen Bay include nutrients (nitrogen, phosphorus), COD, and petroleum hydrocarbons, whose migration and transformation is studied by this research in seawater. At present, the national seawater quality standards only include indicators for active phosphate and inorganic nitrogen, without indicators for total phosphorus and total nitrogen, which cannot meet the requirement for the calculation of marine environmental capacity and pollution control in the sea area. Consequently, this research aims to control total nitrogen and total phosphorus, and adopts the method of on-site measurement of total nitrogen, total phosphorus, inorganic nitrogen and inorganic phosphorus content in seawater and sewage, based on which the new method is used to determine the ratio of total nitrogen to inorganic nitrogen and the ratio of total phosphorus to inorganic phosphorus in seawater and sewage, solving the problem of missed indicators for nutrient biochemistry migration and transformation in numerical model calculations. The ratio of inorganic nitrogen to total nitrogen and ratio of active phosphate to total phosphorus in Xiamen Bay is 0.621 and 0.412, respectively; The control concentrations of total nitrogen and phosphorus in Xiamen Bay under the three types of seawater quality standards are 0.999mg/L and 0.055mg/L, respectively. For the study of the migration and transformation of COD in the bay, this research has adopted the COD degradation kinetics equation: firstly, the relationship between the degradation rate of constant k and seawater temperature is established, and the degradation rate constant of COD in Xiamen Bay is calculated to be 0.05/d; Then, according to the first-order degradation kinetics relationship of COD $C=G_0e^{-Kt}$, the degradation kinetics equation of COD in Xiamen Bay is $C=C_0e^{-0.05t}$. To calculate the migration and transformation of petroleum hydrocarbons in the bay, this research adopts the natural weathering mode of petroleum hydrocarbons in estuarine harbors. Based on the relationship among degradation rate constant, temperature, and salinity, the degradation rate constant of petroleum hydrocarbons in Xiamen Bay is calculated to be 0.009/d, and the migration and transformation of petroleum hydrocarbons can be expressed as $C=C_0/(0.0091tC_0^{0.1}+1)$; Finally, the research results in this paper are applied to the numerical calculation of environmental capacity in Xiamen Bay [30].

One of the representative international research on ocean circulation models is ROMS currently widely used, which has been adopted by Li Yuxuan (2024)[31]. A high-resolution ocean dynamics model covering the North Pacific area was established based on ROMS. In combination with passive tracing experiments, the distribution of radioactive nuclides emitted into the sea from the Fukushima Daiichi nuclear power plant was simulated over the period of 5 years. The results indicated that after being discharged into the sea, radioactive nuclides mainly moved eastward with the Kuroshio Extension, but there were still some radioactive nuclides reaching the offshore waters of China in a southwest direction due to southwest reflux, vortex activity and modal water submergence processes. In addition, ROMS has been currently used in the environmental impact assessment of radioactive nuclides emitted from the Fukushima Daiichi nuclear power plant accident by Tokyo Electric Power

Company in Japan. The model has been validated by using environmental monitoring values of cesium activity concentration in seawater [31][39].

Another environmental impact assessment modeling against Fukushima Daiichi nuclear power plant accident is conduced by Zhao yunxia et al., (2024) [32], based on the complete set of Earth's fluid dynamics control equations from the First Institute of Oceanography of the Ministry of Natural Resources, who choose the schemes of both before and after Euler difference and combine both forward and inverse duality space smoothing to develop the three-dimensional ocean circulation numerical model, MAS NUM. This model is the world's first ocean circulation model by using a dual time layer visualization format, also becoming one of the more advanced third-generation ocean numerical models in the world, whose results have been validated and applied currently. Zhao Yunxia et al., (2024) combined MASNUM model with the radioactive nuclide transport model proposed by Perianez et al., [33] against the Fukushima Daiichi nuclear power plant accident, by establishing a regional transport and diffusion model of radioactive nuclides in the northwest Pacific without considering marine sedimentation, which simulated the diffusion behavior of 137Cs in the region over a 20-year period [32][39].

Based on the establishment of a Pacific hydrodynamics model, it was to explore the diffusion law of nuclides in the relevant sea area after the accident of the Fukushima nuclear leakage, calculating the predicted discharge of Fukushima nuclear wastewater by ship and the predicted discharge of nuclear wastewater from a tunnel at 1 km away from the coast. By comparing the calculated results with the actually measured values, it was found that the modeling results were in good agreement with the measured values, proving the accuracy of the calculated results. The calculation results indicated that nuclear-contaminated water migrated with ocean currents, while it diffused naturally. Radioactive nuclides that were emitted from the areas with high concentrations migrated northward along the coastline and then spiraled northeastward. After the discharge of nuclear-contaminated water by ship, the migration of nuclides with ocean currents was relatively slow, mainly showing axial diffusion centered on the discharge spot. Subsequently, the radioactive nuclides in nuclear contaminated water were gradually distributed in a band shape due to the influence of ocean currents, tidal currents, and diffusion, which migrated northeastward, arriving in the coastal areas of Japan around the 15th day. Whether it was along the coast or discharged within 1 kilometer, radioactive isotopes could quickly spread to the coast [34][39].

According to the real-time meteorological data, the hydrodynamic model for the nuclide diffusion in the sea area near a nuclear power plant was established by Li Zi Chao et al., (2020), which was based on the Lagrangian method, and the reliability of the model was validated. The hydrodynamic characteristics and nuclide migration paths in the sea area of nearby nuclear power plants were analyzed according to the modeling results, which indicated that the hydrodynamic simulation in the sea area

near the nuclear power plant well characterized the tidal current phenomenon of the semi diurnal tide around this sea area and the basic migration direction of radioactive isotopes started from nuclear power plants and spread northeastward along the coast. Then it was affected by the tidal current, so the nuclide moved forward in rotation. The migration paths of nuclides were different among different seawater layers: surface layer nuclides migrated along the coast, with the closest migration distance, and middle layer nuclides were farther away from the coast, with the farthest migration distance, while bottom layer nuclides migrated at the distance between surface and bottom layer nuclides [35].

Another research conducted by Li Zi Chao et al., (2020) studied the migration and diffusion laws of radioactive nuclides in nearshore areas, which played an important role in emergency decision-making and accident mitigation, under the conditions of nuclear power plant accident event. Based on the AP1000 unit, it was to establish a hydrodynamic model for nearshore sea water in China under the boundary condition of average climate state; Then, according to the six-hour meteorology data of forecasting, the hydrodynamic model specifically for the nuclear power plant located nearby the sea area was established; Finally, by employing Euler's method, the nuclide diffusion model was established, which had been validated. According to the modeling results, the migration pattern of nuclides in the vicinity of the nuclear power plant was analyzed after a nuclear leakage accident, showing that the hydrodynamic model for the sea area near the nuclear power plant well characterized the flow field of the seawater around the nuclear power plant, and the difference between the simulated water level and the measured water level was controlled within 10cm over the seabed foundation; It was found that the migration direction of ^{131}I in the vicinity of the nuclear power plant was basically consistent with that of ^{137}Cs, and both nuclides species migrated eastward along the coastline and diffused southward; For the emergency response to nuclear accidents, the effect of the longer half-life decaying nuclide ^{137}Cs on the radioactive activity could be disregarded, but the decay of the short-lived nuclide ^{131}I resulted in the significant impact on its radioactivity [36].

Another notable type of marine pollution species is organic pollutants. For example, frequent oil spills and coastal land-based oil pollution can cause both short-term or long-term degradation to marine ecosystems. Biochar is a kind of material that is rich in carbon with a wide range of raw material sources, low cost and environmental friendliness. It is an important measure to solve the global waste carbon footprint problem, and marine petroleum hydrocarbon remediation materials based on biochar have received widespread attention in recent years [37]. Due to the air-sea circulation, the organic marine pollutants in marine ecosystem can re-enter the atmosphere. For example, in recent years, the rate of warming in the Arctic has been almost twice than the global average rate of warming, and the accelerated melting of sea ice releases persistent organic pollutants (POPs) from sediments back into the atmosphere [38].

8.2. Discussion

Table 2. Summary of ocean pollution research.

Location	Pollutant species	Measuring method	Modeling
Xiamen Bay [30]	total nitrogen, total phosphorus, inorganic phosphorus	On-site measuring	
	COD		Quantifying the relationship between the degradation rate of constant k and seawater temperature; The first-order degradation kinetics relationship of COD; Quantifying the relationship among degradation rate constant, temperature, and salinity
Fukushima Daiichi nuclear power plant [31]	radioactive nuclides	environmental monitoring values of cesium activity concentration	Ocean circulation models of ROMS
Fukushima Daiichi nuclear power plant [32]	radioactive nuclides		A combination of MASNUM model and radioactive nuclide transport model proposed by Perianez et al., [33]
The discharge of nuclear-contaminated water by ship from Fukushima Daiichi nuclear power plant [34]	radioactive nuclides	actually measured for model validation	Pacific hydrodynamics model
The sea area near a nuclear power plant [35]	the nuclide diffusion		the hydrodynamic model based on the Lagrangian method;
The sea area near a nuclear power plant[36]	radioactive nuclides: ^{131}I, ^{137}Cs		the hydrodynamic model based on the Euler's method
Ship oil spills and coastal land-based oil pollution[37]	Organic pollutants		

The sediments of sea ice in the Arctic [38]	persistent organic pollutants (POPs)	Monitoring the atmosphere pollutants	

The case studies with regards to the representative ocean pollutant species have been summarized in Table 2, focusing on the radioactive nuclides diffusion in the ocean. It is concluded that the diffusion model of pollutant in seawater can be operated separately in different seawater layer (such as modeling at upper layer, middle layer, bottom layer separately operated by Li Zi Chao et al., (2020)[35]), but the seawater circulation modes must include the seawater circulation between upper layer and lower layers (illustrated by Figure 2, Figure 6, Figure 7 in my article), as well as the seawater circulation at upper layer only (illustrated in 7.1 section of my article), because both seawater circulation modes can significantly influence the ocean pollution transport. In addition, both physical and chemical environment conditions are different among different seawater layers, which may affect the half-life decaying of radioactive nuclides in different ways, so the hypothesis for the future research is that the half-life decaying of radioactive nuclides varies among upper, middle and bottom seawater layers; Further more, the sinking of radioactive nuclides into bottom seawater layer may help to mitigate its environmental impact , because the nuclides may become the sediments on the seabed. Consequently, the discharge of nuclear-contaminated water by ship must select the suitable site with hydrology conditions facilitating the downward seawater flow. For example, the warm seawater concentrated sites pointed out in the Figure 6 and Figure 7 of my conceptional models may facilitate the sinking of radioactive nuclides into bottom layer.

9.Modeling of boundary layer mixing process

9.1.Review of modeling background

Fluid flow is usually classified into Laminar flow and turbulent flow in engineering research. If the trajectory of the fluid particles, which is the function of both initial spatial coordinates (x, y, z) and time t, is a regular and smooth curve, taking the simplest example of a straight line, this flow type is defined as the laminar flow, while the flow without regular trajectory is classified as turbulent flow [40].

Reynolds number (Re) is a dimensionless parameter that can be used to characterize fluid flow conditions, calculated as $Re = \rho v d/\mu$, among which the variables of v, ρ, μ, and d indicate the flow velocity, density, viscosity coefficient of the fluid, and characteristic length respectively. For example, if the fluids flows through a circular pipe, d is estimated as the equivalent diameter of the pipe. The Reynolds number can be used to distinguish whether fluid flow is laminar type or turbulent type, and can also be used to measure the resistance imposed on an object flowing in the fluid substances. When the Reynolds number is small, the influence of viscosity on the flow field is greater than its inertia, and the disturbance of flow velocity in the flow field is attenuated by viscosity, leading the flow to be stable and laminar; when the Reynolds number is large, the influence of inertia on the flow field is greater than that

of viscosity, making the fluid flow less stable, so that small changes in flow velocity are prone to enlarge and enhance, forming the turbulent and irregular flow field [41].

The characteristics of boundary layer mixing process is approximately considered as the isotropic three-dimensional turbulence, with both horizontal and vertical scales ranging from O (10 m) to O (100 m). The current parameterization scheme for the ocean boundary layer is to convert the flux, which is caused by external forcing processes such as wind stress or bottom stress, surface cooling or heating, and solar radiation transmission, into the profile-describing turbulence. The representative modeling programs include KPP (K-Profile Parameterization), Mellor-Yamada programme, GOTM (The Generalized Ocean Turbulence Model）and CVMix（The Community Ocean Vertical Mixing package) [42].

9.2. Design of modeling program

In the section 3 of my article, the philosophy of boundary layer formation simulation is discussed as “the preconditions of boundary layer formation should include two conditions: one is that the spatial variation in substance’s density and composition should reach the threshold, which is reflected by the variation along the spatial scale of modeling; the other is that the relative speed of substance motion is low enough to form boundary layers, which is measured by the variation along the temporal scale of modeling.” Consequently, my article firstly adopts the conception of Reynolds number ($Re = \rho v d/\mu$) to model these two preconditions of boundary layer formation process.

It is to hypothesize that the variable v of flow speed is defined as the flow speed within boundary layer that is formed between upper layer and lower layer. Then the variable v of flow speed is affected by the relative speed of substance motion. If the relative speed of substance motion between upper and lower layers is slow, the variable v of flow speed within boundary layer is also slow due to the reduced driving force caused by the less speed variation between upper and lower layer; If the relative speed of substance motion between upper and lower layers is quick, the variable v of flow speed within boundary layer is correspondingly accelerated due to the increased driving force caused by the higher speed variation between upper and lower layer; Then it is to hypothesize that variable d of characteristic length indicates the vertical thickness of boundary layer, which is influenced by the relative speed of substance motion as well. If the relative speed of substance motion between upper and lower layers is slow, the vertical thickness of boundary layer is short due to the sinking effects of more stable flow field; If the relative speed of substance motion between upper and lower layers is quick, the vertical thickness of boundary layer is longer due to the mixing effects of more turbulent flow field; Finally it is to further hypothesize that variable μ represents the viscosity coefficient of the fluid within boundary layer, which is affected by the spatial variation in substance’s density and composition. To simplify the calculation process in ocean water environment, the spatial variation in substance’s density and composition is quantified by both salinity and temperature

variation between upper and lower layers. The higher spatial variation in both salinity and temperature between upper layer and lower layer will result in the heterogeneity of substances, increasing the friction coefficient between them, so that the viscosity coefficient of the fluid within boundary layer is increased correspondingly. Of course, if it is to simulate this process in atmospheric or geological environment, the spatial variation in both salinity and temperature may be changed into other parameters that are conveniently available and easily measured to indicate the spatial variation in substance's density and composition. Consequently, this modeling program is expressed as:

Equation 1: Variable $v = f(\Delta v)$

where the variable v of flow speed within boundary layer is the function of Δv, and Δv is the relative speed of substance motion between upper and lower layers, which is positively correlated with variable v.

Equation 2: Variable $d = E(\Delta v)$

where the variable d of vertical thickness within boundary layer is the function of Δv, which is positively correlated with variable d.

Equation 3: Variable $\mu = \partial(\Delta S, \Delta T)$

where the viscosity coefficient of the fluid (μ) within boundary layer is the function of both ΔS and ΔT that are the salinity variation and temperature variation between upper and lower layers, respectively. Both ΔS and ΔT are positively correlated with the viscosity coefficient of the fluid (μ).

Equation 4: $Re = \rho vd/\mu$

Then the equation 1, 2 and 3 is integrated into equation 4. Obviously, the numerical modeling reflects that the slower relative speed which indicates more stable flow field, or the higher spatial variation in both salinity and temperature which leads to higher friction coefficient will result in smaller Reynolds number (Re), representing laminar flow; the quicker relative speed which indicates more turbulent and mixing flows, or the smaller spatial variation in both salinity and temperature which leads to smaller friction coefficient will result in higher Reynolds number (Re), representing turbulent flow. Consequently, this correlation among different variables in my modeling is reasonable in both theory and engineering practice.

When this modeling program is applied, the empirical data, including seawater temperature, seawater flow speed, density and seawater salinity, are required to quantify the relationship in above equations, deriving the parameters. There is an

example of 3-dimension numerical modeling of boundary layer formation process which is built by using C++ languag according to assumed data in the Appendix.

10.Conclusion

In my previous article [1], by comparing and contrasting the formation mechanism of tornadoes and geological faults with ocean hydrology, it is proposed that the sudden breaking of ocean water boundary layers will result in the vortex turbulence flow, including tsunami wave, which may be triggered by the factors such as strong wind, alteration of seabed topography, earthquake occurrence under seabed, etc.

My article has substantially discussed the new theories and methods in responses to the three hypotheses proposed at the beginning of this research project. Firstly, seawater boundary layer is essential to analyze the complex hydrology of ocean circulation, which is especially the key to reveal the seawater circulation between upper seawater layer and lower layer; Secondly, sea-air interaction makes the seawater become the adjuster to influence the climate change, especially including precipitation and global warming; Thirdly, the seawater boundary layer plays significant role in analyzing the ocean pollution transport and mitigation, especially for the solution of nuclides wastewater discharge. This article has also aimed to build a model to simulate the boundary formation process by adopting Reynolds number calculation, but each variable of Reynolds number equation is modified and re-defined with full discussion of its rationale.

Please note: The whole workflow of this research, including unfinished manuscripts updated, figures, dataset and final version of preprint, is posted in the open science platforms (OSF, Zenodo and Researchgate) before formally publishing, for the purpose of receiving external feedback, as the peer review process. The data-sets drawing Figure 3, 4, 5, 8, 9,10 and software are uploaded in Zenodo together with formally published manuscript.

References:

1. Liu Huan. (2021). Discussion of The Formation Mechanism of Tornadoes and Geological Faults. Journal of Environment and Health Science (ISSN 2314-1628), 2021(06). https://doi.org/10.58473/JAES0006
2. Liu Huan. (2021). Ancient Chinese Eight Diagrams and Application on Chemistry Reaction Rate. Journal of Environment and Health Science (ISSN 2314-1628), 2021(02). https://doi.org/10.58473/JQPMC0010
3. Liu Huan. (2021). The formation mechanism of substance boundary layers. Journal of Environment and Health Science (ISSN 2314-1628), 2021(2). https://doi.org/10.58473/JAES0004
4.海洋水文要素。搜狗百科。
5.海水温度。搜狗百科。
6.海洋潮汐。搜狗百科。
7.海流。搜狗百科。
8.科里奥利力。搜狗百科。
9.地球洋流。搜狗百科。
10.密度流。搜狗百科。
11.风海流。搜狗百科。
12.地转流。搜狗百科。
13.漂流理论。搜狗百科。
14.离岸流。搜狗百科。
15.补偿流。搜狗百科。
16.风生海流。搜狗百科。
17.Liu Huan (2024). Original Review of Environmental Physiology: Photosynthesis and Systematic Metabolomics. Journal of Biological Sciences (ISSN 2958-4035).2024(07). https://doi.org/10.58473/JBS0024
18.海洋。搜狗百科。
19.齐庆华,靖春生.菲律宾海水文动力环境分析及对海洋生态区划的启示[J].海洋开发与管理,2022,39(08):44-49.DOI:10.20016/j.cnki.hykfygl.20220706.002.
20.丛帅,刘时桥,辛姿仪,等.台风“巴蓬”对南海上层海洋水文特征与生态环境的影响[J].海洋地质前沿,2022,38(10):79-86.DOI:10.16028/j.1009-2722.2021.174.
21.叶海军，唐丹玲，潘刚. 强台风鲶鱼对中国南海浮游植物及渔业资源的影响[J].生态科学，2014，33(4)：567-663.
22.管守德,侯一筠.西北太平洋超强台风 Tembin(2012)引起的海表面降温与强混合研究[J].海洋与湖沼,2020,51(06):1301-1309.
23.Glenn S M, Miles T N, Seroka G N et al, 2016. Stratified coastal ocean interactions with tropical cyclones. Nat Commun, 7(1): 10887.
24.Guan S D, Liu Z, Song J B et al, 2017. Upper ocean response to Super Typhoon Tembin (2012) explored using multiplatform satellites and Argo float observations. Int J Remote Sens, 38(18): 5150—5167.
25.周慧,杨文龙,刘恒昌,等.台风“海马”对吕宋海峡附近暖涡的影响及其动力机制[J].海洋与湖沼,2017,48(06):1276-1288.
26.竺婧.北半球夏季海洋性大陆区域海温异常特征及与亚澳地区气候异常的联系[D].南京信息工程大学,2023.DOI:10.27248/d.cnki.gnjqc.2023.000011.

27. Liu Huan. (2021). Discussion of Tornado Formation Mechanism. Journal of Environment and Health Science (ISSN 2314-1628), 2021(08). https://doi.org/10.58473/JAES0007
28. 宣莉莉.热带东印度洋上层海洋环流及其与孟加拉湾水交换的季节变化研究[D].国家海洋局第三海洋研究所,2013.
29. 张丽萍.全球变暖背景下水循环变化对海洋环流及气候的影响[D].中国海洋大学,2012.
30. 崔江瑞.污染物在海洋中的迁移转化及其在海湾环境容量研究中的应用[D].厦门大学,2009.
31. 李宇轩,赵昌,杨德周,等.福岛以东放射性核素进入中国海关键途径的三维数值模拟研究[J].原子能科学技术,2024,58(10):2008-2021.
32. 赵云霞,韩磊,曲大鹏,等.福岛核事故释放的137Cs在西北太平洋海水中输运的模拟与预测[J].海洋科学进展,2017,35(02):221-233.
33. PERIANEZ.R, ABRIL J. M, GARCIALEON M. Modelling the dispersion of non-conservative radionuclides in tidal waters, Part 1: Conceptual and mathematical model[J]. Journal of Environmental Radioactivity, 1996, 31(2): 127-141.
34. 周涛,许鹏,毛赏,等.福岛核污水排放预测计算研究[J].核科学与工程,2023,43(02):451-460.
35. 李子超,周涛,司广成,等.基于拉格朗日方法的核素近海迁移计算[J].核动力工程,2020,41(02):72-77.DOI:10.13832/j.jnpe.2020.02.0072.
36. 李子超,周涛,司广成,等.基于欧拉方法的核素近海迁移计算[J].核科学与工程,2020,40(02):256-263.
37. 孙晓军,付红蕊,包木太,等.生物炭材料在海洋石油类污染修复中的应用研究进展[J].环境化学,2023,42(03):1029-1041.
38. 胡成格,刘鸿伟,谢周清.北极大气中典型持久性有机污染物对海冰变化的响应[J].第四纪研究,2021,41(03):780-791.
39.刘森林,吴仁杰,张欣钰,等.放射性核素生态运移与辐射剂量评价研究现状及趋势[J].原子能科学技术,2024,58(10):1989-2007.
40.层流与湍流。搜狗百科。
41.雷诺数。搜狗百科。
42.谢经纬,刘海龙,郑伟鹏,等.全球海洋环流模式研究进展[J].地球科学进展,2024,39(05):454-465.
43. Liu Huan (2021). Modeling of annual net primary production of a forest in the Taramakau Valley, Westland, New Zealand. Journal of Environment and Health Science (ISSN 2314-1628). 2021 (02). https://doi.org/10.58473/JEHS0007

Appendix. An example of numerical modeling of boundary layer formation.

The axes of this 3-Dimension numerical model include x, y, z axis in 3-dimensional space; Δv is defined as X[i][j][k], where i, j, k is the spatial grid number in x, y, z axis respectively; ΔS and ΔT is expressed as Y[i][j][k] and Z[i][j][k] respectively, where i, j, k is the spatial grid number in x, y, z axis respectively; R[i][j][k] is the Reynolds number (Re =ρvd/μ), where i, j, k is the spatial grid number in x, y, z axis respectively. In this example, in total 3×3×3 spacial grids are assumed in the x,y,z axes; Equation 1 is assumed to be Δv ^ n; Equation 2 is set to be e ^ Δv; Equation 3 is set as 3*ΔS*ΔT. Each value in X[i][j][k], Y[i][j][k] and Z[i][j][k] is assumed and input into X[3][3][3], Y[3][3][3], Z[3][3][3] (this means that in total 3×3×3 spacial grids in the x,y,z axes). Density ρ and parameter n is assumed to be 2. Please note: the starting number of spatial grid along x, y, z axis is zero, and the max number of spatial grid along x, y, z axis is 2 in this example (in total 3×3×3 spacial grids). Similarly, if the total amount of spatial grids is set as i × j × k in the x, y, z axes respectively, then the starting number of spatial grid along x, y, z axis is zero and the max number of spatial grid is (i-1), (j-1), (k-1) along x, y, z axis respectively. Then this numerical modeling is edited as:

```
#include<iostream>
#include<math.h>
using namespace std;

int main ()
{
    int i=0,j=0,k=0;
    float R[i][j][k],n=2.0,e=2.718;
    float X[3][3][3]=
    {
        {{1,1,2},{1,2,3},{2,3,4}},
        {{5,6,7},{8,9,10},{11,10,9}},
        {{11,9,10},{15,16,17},{11,15,9}}
    };

    float Y[3][3][3]=
    {
        {{1,1,2},{1,2,3},{2,3,4}},
        {{5,6,7},{8,9,10},{11,10,9}},
        {{11,9,10},{15,16,17},{11,15,9}}
    };

    float Z[3][3][3]=
    {
        {{1,1,2},{1,2,3},{2,3,4}},
        {{5,6,7},{8,9,10},{11,10,9}},
```

```
        {{11,9,10},{15,16,17},{11,15,9}}
    };

        for(int i=0;i<3;i++)
        {
            for(int j=0;j<3;j++)
            {
                for(int k=0;k<3;k++)
                {

R[i][j][k]=2*(pow(X[i][j][k],n))*(pow(e,X[i][j][k]))/(3*((Y[i][j][k])*(Z[i][j][k])));

cout << "Element at R["<< i<< "]["<<j<<"]["<<k<<"]=" << R[i][j][k] << endl;

                }
            }

        }

        return 0;

}
```

Further discussion: if the real empirical data are available, the parameterization process of each equation (equation 1, 2, 3) will be conducted to estimate the necessary parameters, after which the sensitivity analysis for each parameter must be tested and the sensitivity analysis method has been illustrated in detail by my another numerical modeling article [43].